The Impact of Turbulence and Turbine Operating Condition on the Wakes of Tidal Turbines

T Ebdon, M Allmark, D O'Doherty A Mason-Jones, T O'Doherty
Cardiff Marine Energy Research Group, Cardiff University, Cardiff

G Germain and B Gaurier
IFREMER, Marine and Structures Laboratory, Centre Manche Mer du Nord, Boulogne-sur-Mer

ABSTRACT

Before initiating a study on the interaction of multiple wakes, it is imperative that turbine wake hydrodynamics are studied in isolation. In this paper CFD computer simulations of downstream turbine wakes have been run using a scale-resolving hybrid turbulence model known as a detached eddy simulation. To allow validation of the CFD simulations the computer models were supported by flume measurements with a lab scale tidal stream turbine run at three tip-speed ratios and three turbulence conditions, varying both turbulence intensity and length-scale.

From the study it was demonstrated that turbulence intensity has a significant impact on the wake development for both recovery and width. The turbulence length scales of between 0.25 and 1.0 rotor diameter did not have a significant impact on the wake.

The turbine operating condition also had an impact on the resulting wakes. In the near wake, centreline velocity recovery was found to increase with increasing turbine thrust due to flow being diverted towards the turbine nacelle. For a volumetric averaged wake, greater power extraction was found to cause the greatest near-wake deficit. Wake width was found to increase with increasing tip-speed ratio (and therefore turbine thrust).

Keywords: Turbine Wake characteristics, Turbulence, Tip speed ratio, CFD modelling, Experimental analysis.

1. INTRODUCTION

As with many industries reliant on the exploitation of fluid flows, the tidal stream turbine industry has used a combination of numerical modelling and scale testing in order to reduce the financial risks involved in installing full-scale turbines at tidal sites [1-5]. Much of the numerical modelling of tidal turbines has examined a diverse range of factors from blade design to flow-misalignment to ambient turbulence and their impacts on turbine performance [2, 3, 5]. Largely due to the computational costs associated with large, detailed models of turbines, the majority of this work has concentrated on the performance of individual, isolated turbines. In order to most effectively exploit the tidal stream resource, which is found in areas of limited geographical extent, tidal turbines are expected to be deployed in arrays, and the close proximity of turbines to one-another in these arrays has the potential to lead to interactions between them. In contrast to the wind, the tidal resource is highly predictable in both speed, direction and temporal variations [4]. Therefore, there is more potential for optimisation in the array layout of tidal stream turbines, by minimising detrimental interactions and maximising positive interactions between the turbines. In order to achieve this end, it is crucial to improve the current understanding of the physical processes occurring in the wake of tidal stream turbines by exploring what factors influence the size and shape of the wake, and what is the nature of the turbulent flow in the wake region. Knowledge of this will inform array layout, allowing the right compromises to be made in order to maximise energy extraction whilst

reducing turbine loading and capital costs, and minimising any potential impacts that turbine arrays might have on the wider environment. This can be achieved by building confidence in a numerical model of turbine wakes through validation against flume experiments and/or full-scale models and prototypes. These models can subsequently be used to explore a wider range of conditions experienced by the turbines to increase understanding of the interaction of wakes and turbines, leading to optimised array designs. To date, most modelling of tidal turbine wakes has been conducted using Reynolds-Averaged Navier-Stokes (RANS) turbulence models or vortex methods [1], however, these have been shown to overpredict the extent of the wake when compared to experimental measurements [6, 7], demonstrating the need for a different approach.

1.1 Wakes of isolated turbines

Early work on wake development was conducted by Lissamann [8] and Jensen [9]. Frandsen et al. [10] adapted the work of Jensen and applied it to arrays of offshore wind turbines. The 'top-hat' profile, which underestimates velocity deficit at the centre of the wake and overestimates it at the wake edges, was replaced by Bastankhah and Port´eAgel [11] with a Gaussian profile. Lam and Chen [12] combined axial momentum theory across an actuator disc with flume measurements from Maganga et al. [13] to develop analytical equations for the prediction of the axial velocity deficit and its lateral distribution downstream of a tidal turbine which were later adapted to include the effects of the turbine hub and predict the region of "double-dip" wake deficit seen in the near-wake region [14]. The improved equations showed good agreement with measurements made by Mycek et al. [15]. One of the earliest studies of the wake of a tidal turbine was conducted in a flume experiment by Maganga et al. [13]. They found that the turbulence intensity (TI) had a significant effect on the length of the wake.

Early numerical studies sought to reduce computational expense through the use of porous discs to simplify the geometry of a turbine, whilst still producing a wake. Models have been presented by Harrison et al. [16], Malki et al. [17] and Bai et al. [18], amongst others, which all combine an actuator disc approach with RANS-based CFD modelling for the flow field around and downstream of the disc. These steady-state models however fail to capture the transient effects in the near wake. Attempts to make the actuator disc model more closely match a physical turbine have been made by Nishino and Willden [19], to account for turbulence from the turbine blades, to more accurately reproduce the near wake mean flow.

Measurements have been made in the wakes of actuator discs [20] and in some cases behind individual turbines [13, 21, 22]. The work of Maganga et al. [13] showing that an increase in TI causes faster wake recovery, was confirmed by Mycek et al. [21], who concluded that, whilst an increase in ambient TI only had a limited effect on the mean power coefficient (C_P) and thrust coefficient (C_T), the wake was "deeply influenced" by the upstream turbulence, and that the "wake shape, length and strength largely depend on the upstream turbulence conditions". Investigations into the turbulence produced in the near wake (between 1.5 and 7 diameters downstream of the rotor) were made by Tedds et al. [23] who noted that the rotation of the turbine blades induced significant anisotropy into the turbulence, and suggested that numerical models which rely on the assumption of isotropic turbulence may struggle to accurately reproduce the flow.

1.2 Interactions within small groups of turbines

As with studies on the wakes of single turbines, much of the initial research into blockage effects used actuator discs, either experimentally or using (Blade Element Momentum-CFD) BEM-CFD models [19, 24]. Turnock et al. [25] used a coupled BEM-CFD model to examine the effects of turbine separation both laterally and longitudinally. They found that a lateral spacing of 2 turbine diameters provided the highest power output from a row of turbine. This has been supported by other studies using a BEM-CFD method [18, 26] and with full-rotor

RANS CFD [27]. These studies found that lateral spacing of 2.5*D* [18] (where *D* represents the diameter of a turbine) and 2*D* [26, 27], gave the highest C_P for turbines in this row. It was also found that a second row of turbines should be at least 5*D* downstream of the first row and staggered for the best overall performance [27].

The effects of lateral and longitudinal spacing on the wakes of tidal turbines has been studied by Stallard et al. [28]. The study found that for lateral spacing ≥3*D*, the wakes of the individual turbines are unchanged from the case of an isolated turbine, but for spacing of ≤2*D* the wakes from the individual turbine merge to form one single wake by 4*D* downstream of the rotors. Another study, this time using PIV measurement techniques, demonstrated the complex nature of turbine interactions within an array [29]. This found that the lateral spacing between turbines effected the array centreline wake recovery, potentially having a detrimental impact on downstream turbines. Field tests of multiple turbines have also been conducted to examine the interactions between turbines and the dependence on turbine spacing by measuring the change in C_P due to the presence of a second turbine [30]. The study examined both lateral and longitudinal spacing of two identical turbines, finding that lateral a spacing of 2*D* produced a performance increase of up to 6%. Due to the restrictions on the towing rig used, a maximum longitudinal spacing of 6*D* was measured, which revealed a 59% reduction in performance, However, when the downstream turbine was offset by 1.5*D* or 3*D* from the centreline of the upstream turbine, no negative effects were observed, giving an idea of the effective width of the wake.

Other studies have examined the rate of wake recovery behind the turbine, both numerically and experimentally [6, 13, 31, 32]. Examining the length of the wake's feeds into considerations of longitudinal spacing of turbines within arrays. An increase in ambient turbulence causes faster wake recovery [13, 20, 33-35]. Hence the position of a downstream turbine will be dependent on the wake-length and width of an upstream turbine. However, the characteristics of the turbulence is also important [13, 32]. As mentioned above, the anisotropy in the wake induced by the turbine [7, 36, 37] has been investigated in the context of arrays [27, 36] and found to have notable influence.

2 WAKE ANALYSIS METRICS

The length, width and characteristics of a wake are dependent on the shape of an object in the flow [38], the nature of the flow and the fluid itself. The wake induced by the presence of the object is a region of slower moving fluid with increased turbulence when compared to the free-stream (Figure 1). Mixing takes place between the higher velocity free-stream and the lower velocity wake, and the associated change in momentum causes the wake to gradually return to the same velocity as the free-stream. This is known as wake recovery. Just behind the object, the lower velocity wake and higher velocity free-stream regions are distinct from one another, separated by a thin, highly sheared layer; flow recirculation is often observed in this near wake region. As the fluid progresses downstream, momentum exchange takes place across the shear layer, leading to wake recovery taking place from the outside towards the centre. At the same time, the shear layer becomes thicker, extending outwards into the free-stream and inwards towards the centre of the wake, whilst simultaneously decreasing in strength. The overall area affected by the wake becomes wider, but the strength of the wake itself (the velocity deficit) decreases. At some point downstream of the object, the shear layer reaches the centreline of the wake. Beyond this point, the flow is still affected by the presence of the object upstream, exhibiting increased turbulence and a remaining velocity deficit, but the bounds of the wake become less defined. Eventually, very far downstream of the object, viscous effects will damp down and dissipate any remaining turbulence and the wake will continue to recover, until it is indistinguishable from the upstream flow.

This qualitative description of a wake will be recognised by flow physicists, but in order to compare wakes, quantitative metrics must be developed. Clearly, an area of reduced flow velocity and increased turbulence has the potential to impact downstream turbines through reduced flow velocity and increased turbulence. Whilst the importance of being able to quantify both the strength of the wake as well as the size of the region it affects is clear, developing quantitative metrics by which to do this is more difficult. Developing quantitative metrics is difficult because of the highly turbulent nature of the wake, meaning that the width and length can fluctuate with time [39].

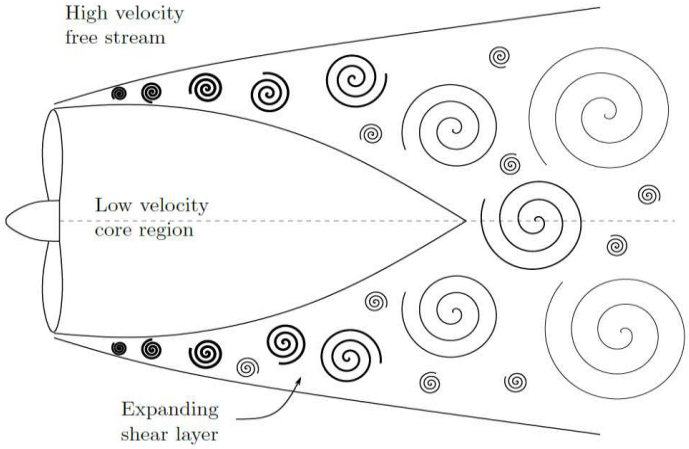

Figure 1: A schematic of the wake description. Flow direction is from left to right.

2.1 Wake length

In general, wake recovery occurs at a higher rate in the near wake, where the difference between the velocities of the wake and the free-stream is greatest, and the exchange of momentum is most effective. As the wake and free-stream become more similar to each other, the effect of momentum mixing reduces, and the rate of recovery decreases and the wake velocity approaches that of the free-stream in an asymptotic manner. For practical measurements of wake length, it is necessary to take a velocity threshold where it can be said that the wake has `recovered'. The choice of this velocity threshold is essentially arbitrary, but for the purposes of this work, a 90% wake recovery (10% deficit) is used. The paper will use terms that are ubiquitous to the subject matter, but the authors will define some of the terms next for clarity.

2.1.1 Centreline velocity recovery

The simplest, and most widely used, method of quantifying the length of the wake is by analysing the recovery of the time-averaged axial velocity along the turbine centreline. This has the advantage of being easily extracted from CFD modelling or measured experimentally. However, it only provides information about the centreline axial velocity, and does not contain any information about the distribution of velocity in the wake region - information of critical importance to turbine and array developers. In addition to this, wake recovery occurs from the outside towards the centreline, meaning that centreline measurements can potentially under-estimate the level of wake recovery since the turbine blades are located some radial distance from the centreline. Using this information alone could lead to a turbine developer using an unnecessarily large downstream spacing for the layout of a turbine array, reducing the amount of energy which can be extracted from a site of limited geographical extent.

2.1.2 Volumetric averaged velocity

To account for the distribution of flow velocity behind the turbine, the volumetrically averaged velocity has also been used. This is an area-weighted estimate of the time-averaged axial velocity through the swept area of the turbine. This was recorded at regular intervals downstream from the turbine and has been shown to give a better estimate of the energy available to a downstream turbine [6]. This is trivial to extract from CFD data; the time-averaged velocity is integrated over the swept area of the turbine at different downstream stations. However, due to the time required to make measurements in a flume, these were only taken on a horizontal plane. To obtain an estimate of the volumetric flow over the swept area of the turbine, a shell (or disc) integration was performed on the measured velocity profiles, following the procedure used by Mycek et al. [21]. The same procedure was also carried out on the CFD data to provide comparative results.

2.1.3 Wake width

Initially, a turbine wake is approximately as wide at the turbine rotor itself. However, as the wake develops downstream, mixing takes place between the high-velocity free-stream, and the lower velocity wake region, causing a layer of sheared flow. Initially this shear is high and the shear layer thin, but as the wake develops, the thickness of this shear layer increases, and the velocity gradient (shear) decreases. This simultaneous change in both thickness and strength of the shear layer makes a simple definition of a wake difficult. This difficulty is only compounded by the fact that the turbine wake may meander in time [33, 35]. Therefore, three different methods have been proposed and used in the analysis of turbine wakes in this paper:

1) a width metric based on the point of maximum-shear,
2) a width metric based on a fixed velocity threshold, and
3) a width metric based on a full-width half minimum method.

All three methods have been designed to be implemented for measurements of time-averaged axial velocity in a rake parallel to the plane of the turbine rotor.

2.2 Wake width based on the point of maximum-shear

In this case the position of the edges of the wake is defined by the point of maximum-shear which is defined as the position with the greatest rate of change in the time-averaged axial velocity in the cross-stream direction. As shown in Figure 2, the wake width is then the distance between the points at which this shear is a maximum.

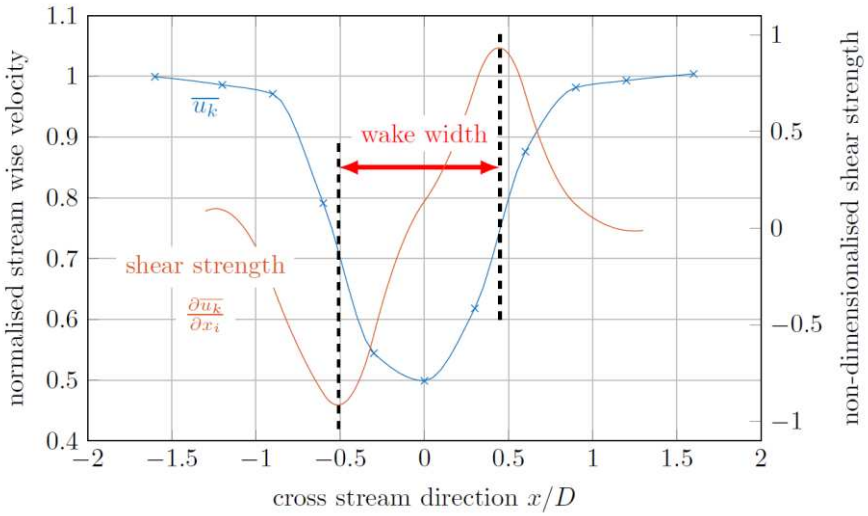

Figure 2: Wake width: the maximum-shear method.

2.3 Wake width based on a fixed velocity threshold

For array designers, a more useful definition of wake width may be the width of the region with a velocity deficit above a certain threshold, i.e. 90% wake as stated earlier (Figure 3). As the wake recovers from the outside inwards due to the mixing of momentum from the free-stream, it is expected that the wake width will decrease as it develops downstream of the turbine. Once all of the wake has recovered to more than 90%, the wake width will become zero [40].

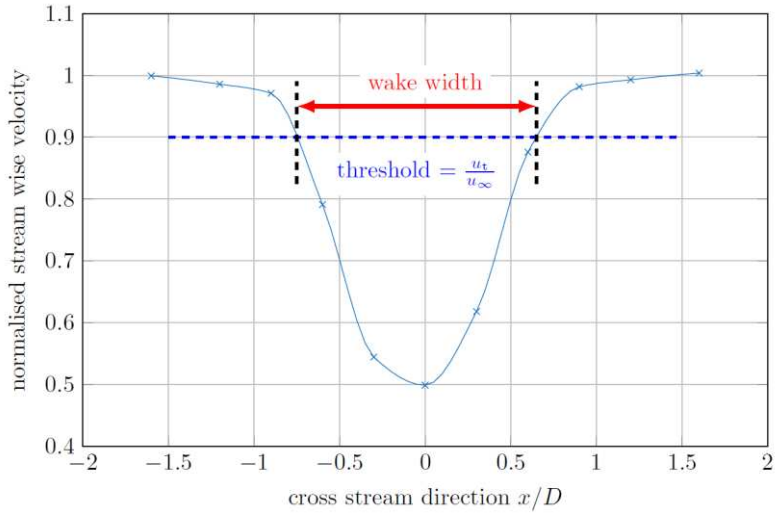

Figure 3: Wake width: the fixed velocity threshold method.

2.4 Wake width based on the full-width half-minimum of the velocity deficit

A third approach, which recognises that the width of the region affected by the wake increases even as the velocity deficit decreases, is taken by a width measurement metric based on the idea of a full-width half-minimum (Figure 4). The full-width half-maximum is a concept often used in statistics and signal processing to analyse the width of a peak. This method is also a velocity threshold, but the threshold at a particular downstream position is chosen as half of the maximum velocity deficit at that downstream position in the wake, rather than being a fixed proportion of the free-stream velocity. Once half of the maximum velocity deficit has been calculated, the width is calculated as the cross stream extent of the wake which has a velocity deficit equal to this value.

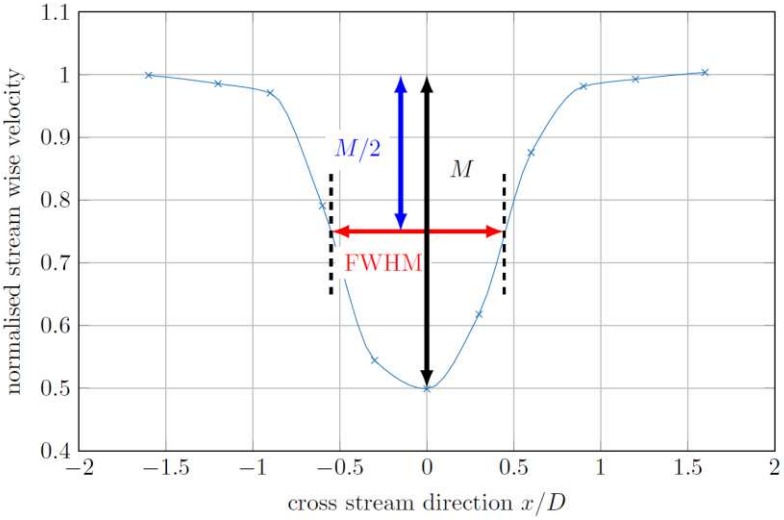

Figure 4: Wake width: Full-Width Half-Minimum (FWHM) method.

3 TURBINE AND EXPERIMENTAL SETUP

The turbine used for this work was a 0.5 m diameter three-bladed, horizontal axis design, with blades based on a Wortmann FX 63-137 section. The blades have a twist of 30° from root to tip and were attached to a 100 mm diameter hub via root stubs and grub screws. The details of the rotor geometry and outputs has been reported in detail elsewhere [6, 37, 41-44]. The turbine nacelle was 763 mm long and a maximum diameter of 160 mm. The turbine hub is directly connected to a Bosch Rexroth type MST130E-0035 synchronous torque motor which is housed within the nacelle along with a slip ring, and associated electronics for control and instrumentation. Electric power and sensor cables are routed out of the downstream face of the nacelle. The motor torque was measured via the electrical current required to either drive or brake the turbine. For all the experiments detailed in this paper, the constant rotational velocity mode was used, replicating the constant rotational velocity used in the CFD study. The turbine assembly is suspended under water by means of a 71 mm diameter stanchion.

3.1 Sensors, data recording and instrumentation

The turbine was designed for physical testing to measure loads on, and power output of a turbine, with a specific focus on condition monitoring [44] but has also been used for work investigating the impact of misalignment [45], and surface waves. Data acquisition (as well as turbine control) was carried out using a National Instruments PXIe-8135 embedded controller and PC. A sample rate of 200Hz was used, which allowed 41s of data to be sampled. This gives a sample rate identical to that from the CFD simulations, with data being sampled over a similar amount of time to the 50s simulated numerically.

3.2 Uncertainty analysis

Uncertainty analysis was conducted for the turbine performance characteristics of C_P, C_T and C_θ. Detailed uncertainty analysis used in the commissioning of the turbine are provided by Allmark [44]. When collecting the data for the power curves presented in this paper, the upstream velocity was not simultaneously measured, but characterised before the tests. Subsequently the flume pump set-point used in the wake measurements was used. Hence, the reference velocity used for the calculation of C_P, C_T and C_θ was based on a mean velocity.

3.3 Flume description

Testing was carried out in the flume facility of the Institut Francais de Recherche pour l'Exploitation de la Mer (IFREMER) in Boulogne-sur-Mer. A description of the flume can be found in [21]. This recirculating flume has a working section 4m wide, 2m deep and with a useable length of approximately 18m. It is capable of flow speeds of 0.1-2.2ms^{-1}, but for turbine testing was only used to a maximum of 1.5ms^{-1}.

3.4 Flow measurement techniques

Flow measurement was made using a 2D DANTEC FiberFLOW two-axis Laser Doppler Velocimeter (LDV) system and calibrated ±0.001 ms^{-1}. The LDV system was attached to a 2D traverse and allowed the measurement procedure to be automated in the cross stream and vertical directions. The measurement positions and times were pre-programmed, allowing measurements to be made for one downstream station (in a plane perpendicular to the turbine axis), before being moved to the next downstream position with errors of the order of ±5 mm. Relative position errors in the cross-stream direction were of the order of ±1 mm.

3.5 Flow conditions

Flume testing was conducted in three stages. Each stage sought to examine the wake under three different types of flow condition; a low turbulence condition (1.75%), obtained using all available flow-smoothing at the tank, and two test sets which used grids constructed of aluminium frames and marine plywood and placed upstream of the turbine to induce turbulence (Figure 5). The dimensions of the grids followed those used by Blackmore et al. [46]. In their

study length scales of between 0.18 - 0.82 m were achieved, approximately 0.35-1.5 times the diameter of the turbine rotor studied in this paper. Using grids about which data had already been published allowed an estimation of the TI and length scales to be expected before going to the flume. The grids were installed by fastening it to the base of the flume and an I-beam above the surface of the water.

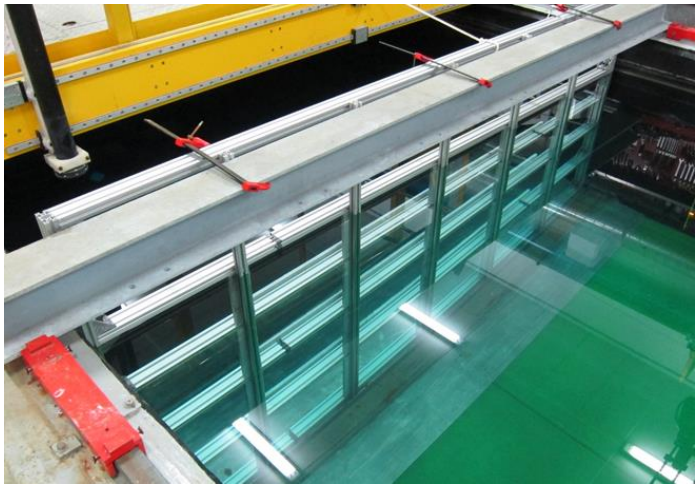

Figure 5: The fine grid installed in the IFREMER flume, viewed from downstream

Before installing the turbine in the flume, the flow downstream of the grid was characterised. This was done via a sequence of LDV measurements in the centre of the cross sectional area of the flume. These were carried out for 1000s each, in order to obtain high confidence in the higher-order statistics. Plots showing velocity, TI and integral length scale (L_T) with distance downstream of the grid are shown in Figures 6a-c respectively for the fine grid, and 6d-f for the coarse grid. Error bars have been omitted from these figures for clarity, as in all cases 95% confidence intervals were less than 0.5% of the values shown. The figures for the fine grid show that the velocity behind the grid increases with downstream distance (most likely due to the near-grid velocity being affected by the position of individual bars, with this effect becoming less influential as downstream distance increases), TI decreases with downstream distance, showing the dissipation of turbulence, and integral length scale tends to increase, indicating the dissipation of the shorter length scales with time. Based on the analysis of flow development behind the grid, as well as consideration of the space required to carry out wake measurements, the turbine rotor was placed at 4m downstream of the fine grid.

The figures for the coarse grid show similar trends to that of the fine grid, albeit as anticipated with a higher TI and greater turbulence length scale. No measurements were made closer than 5m from the grid, as the TI was measured to be over 30% at this point. The turbine was placed 9m downstream of the coarse grid, as this was the greatest distance that it could be placed from the grid, whilst still leaving enough space downstream of the turbine for wake measurements.

Once the centreline measurements had been made and the turbine position chosen, flow uniformity across the swept area of the turbine was assessed by re-measuring at the chosen position on the flume centreline, as well as ±0.25m in both the horizontal and vertical directions, at the limits of the turbine swept area. Each of these measurements was made for 500s and show the flow to be reasonably uniform across the turbine swept area, with the integral length scale being approximately that of the turbine rotor radius behind the fine grid and that of the turbine rotor diameter behind the coarse grid. Turbulence generated from these grids can be expected to be largely isotropic (in the vertical and transverse directions). It is worth noting that turbulence at potential tidal sites is unlikely to be isotropic [47 - 50], however,

the specific turbulence characteristics will be specific to individual sites and would need to be investigated in detail.

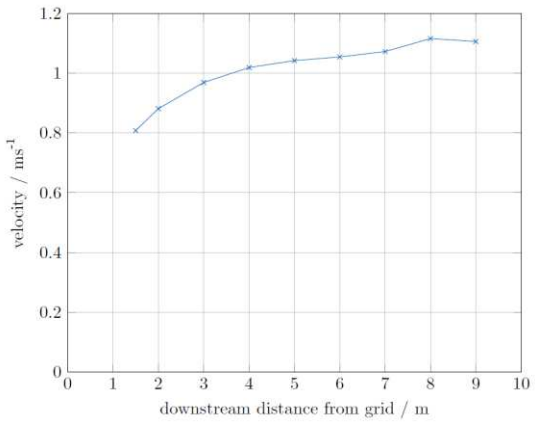

a: Velocity behind the fine grid

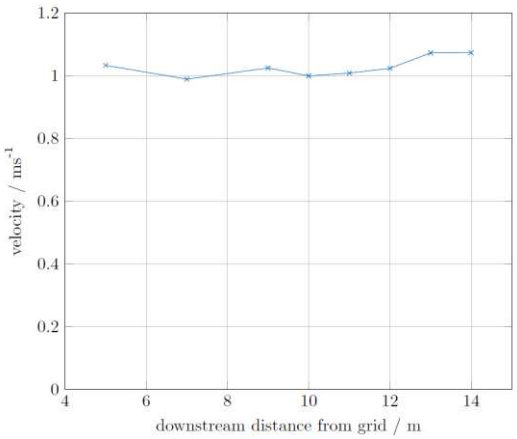

d Velocity behind the coarse grid

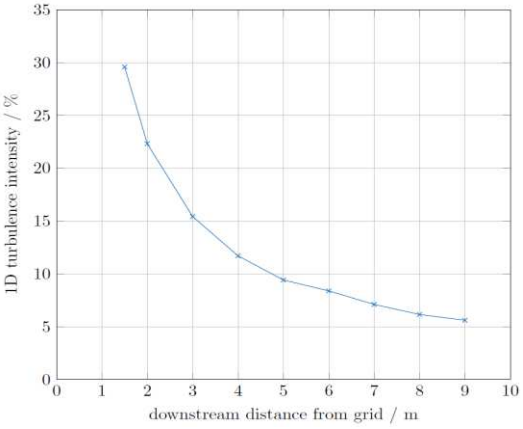

b: 1D turbulence intensity behind the fine grid

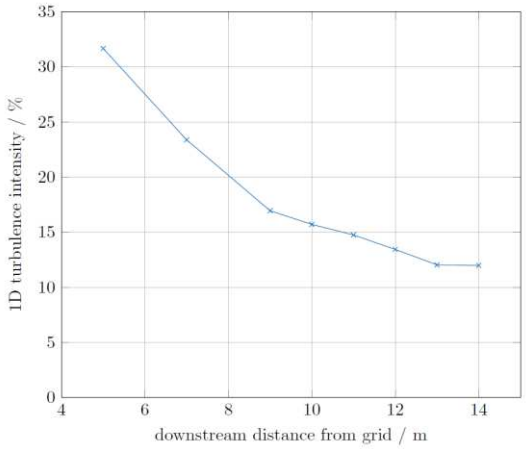

e: 1D turbulence intensity behind the coarse grid

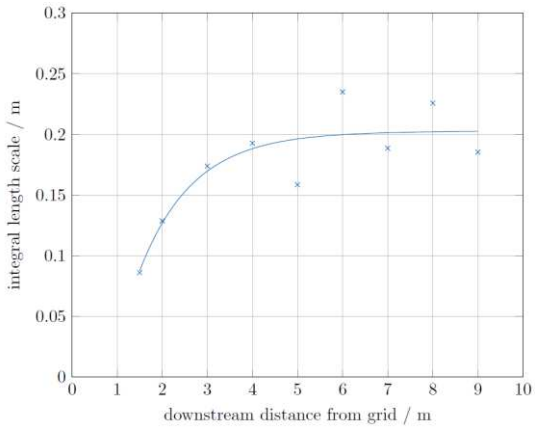

c: Integral length scale behind the fine grid

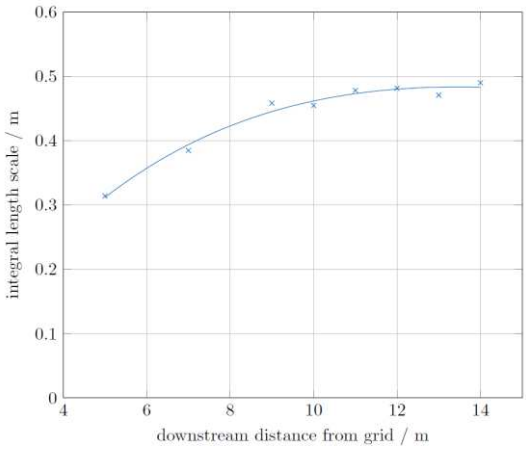

f: Integral length scale behind the coarse grid

Figure 6: Flow characteristics downstream of the fine and coarse grids, measured at the centre of the cross-sectional area of the flume.

For the test conducted in the low turbulence conditions without any grid, vertical profiles of axial velocity and TI were made across the region where the turbine was present. This showed the velocity to vary by ±1.5% and the TI by ≤2% across the diameter of the turbine, indicating a low turbulence, highly uniform flow. A summary of the flow conditions and tip-speed ratios for which wake measurements were made can be seen in Table 1.

Table 1 Test flow conditions at the turbine rotor position.

Grid		**None**	**Fine**	**Coarse**
Distance from grid / m		n/a	4.0	9.0
Velocity / ms^{-1}		1.5	1.02	1.03
1D Turbulence intensity / %		1.75	11.7	17.5
Integral length scale / m		0.5	0.19	0.43
Tip-speed ratios tested	2.5		X	X
	3.65	X	X	X
	4.5		X	X

4. CFD METHODOLOGY

4.1 CFD setup, geometry and boundary conditions

The work contained within this thesis was conducted using the commercial CFD code Ansys Fluent. Fluent uses a finite volume method for solving the continuity and momentum equations for fluid flow. Flume-scale simulations were carried out using Fluent 18.0 on HPC facilities at Cardiff University.

Simulation of the rotating turbine was achieved via a sliding mesh scheme as used by Morris [37]. This involves the creation of two separate domains, with two independent meshes. For the turbine, a cylindrical domain is created within the main domain, encompassing the rotating parts of the turbine. This cylinder is then physically rotated with each timestep, in accordance with the pre-determined rotational velocity. The mesh of the rotating domain and the main domain are not necessarily conformal, and the two meshes slide past each other at the mesh boundaries. This scheme allows for flow interactions between the turbine blades and stanchion and allows these cyclic interactions and the resultant wake to be evaluated.

The turbine was suspended in the centre of the cross-sectional area of a flume, with a width of 4 m and depth of 2 m, giving a blockage ratio by turbine swept area of approximately 2.5%. The CFD domain extended 1.5 m upstream of the rotor, and 7.5 m downstream, representing a modelled domain of from z/D = -3 to z/D = 15. The upstream domain boundary was set as a constant velocity inlet with specified turbulent conditions, including the addition of synthetic turbulent perturbations. Inlet turbulence was specified via turbulence intensity and a length scale, described by Ansys as representing the length scale of the turbulence features containing the most energy; similar to the definition of the integral length scale [46]. Production of turbulence perturbations using this method is based on a Biot-Savart rule, and 1000 seed vortices were chosen, in keeping with the Ansys recommendation that the number of seed vortices should be approximately ¼ the number of cell faces at the inlet.

The downstream domain boundary was a constant pressure boundary with a gauge pressure of 0 Pa. A zero-shear condition was applied to the upper domain boundary rather than representing a free surface, in common with other low-blockage numerical simulations. All other boundaries (both flume walls and turbine) were treated as stationary no-slip walls, using the default roughness coefficient of 0.5.

A comprehensive mesh independence study was carried out by varying the mesh densities in the area immediately around the turbine rotor, the nacelle region, the wake region, and the

surrounding volume of fluid. The resulting mesh contained a total of 11.38*10^6 cells and is detailed in [51].

4.2 Turbulence model

To date, the majority of numerical research on tidal turbines and their wakes has been conducted using RANS turbulence models. These models recognise that, for most engineering flows, users are more interested in the time-averaged values of flow variables such as velocity, than the instantaneous values. RANS models are based on the idea that the instantaneous value of a flow variable, e.g. velocity, can be represented by its mean and a fluctuating component. This process is known as Reynolds decomposition, and is represented mathematically in equation 1, where U is the time-averaged flow velocity, and $u'(t)$ represents the fluctuating component of velocity.

$$u(t) = U + u'(t) \qquad (1)$$

The Reynolds-decomposed variables are then substituted into the incompressible 3-dimensional Navier-Stokes equations. This yields the time-averaged Navier-Stokes equations for U, which are formally identical to the Navier-Stokes equations for instantaneous flow variables, with an additional term, shown in equation 2, and known as the Reynolds stresses. Here u'_i and u'_j represent instantaneous velocity components in the I and j directions respectively, ρ represents density, and τ_{ij} represents the tensor stress component in the ij direction.

$$\tau_{ij} = -\rho\overline{u'_i u'_j} \qquad (2)$$

The Reynolds stresses represent the exchange of momentum between the mean and the fluctuating flow components, and must be modelled in order to close the Navier-Stokes equations and obtain a solution for U. Various schemes have been developed for the modelling of the Reynolds stresses, each with differing levels of complexity, from the mixing length model, through two-equation models such as the k-ε and k-ω through to the Reynolds Stress Model, which requires seven equations to be solved for closure to be achieved [52].

The advantage of RANS equations is that they provide a good compromise between computational cost and accuracy. They are well characterised, and it is known which ones perform best for different types of flow. Variations such as the k-ω SST model exist, which attempt to combine the best characteristics of the k-ε and k-ω models. However, these models struggle with flows which demonstrate a large turbulence length scale or a high degree of turbulence anisotropy like that shown to be present in the wake of a tidal turbine [23]. This is thought to be due to the reliance of two-equation RANS models on the Boussinesq approximation, which assumes isotropy of turbulence. This assumption is usually valid for small-scale turbulence, but it becomes less appropriate for larger turbulent length scales [48], such as those found at potential tidal energy sites [53]. In addition to this, the focus on time averaged values means that some data regarding fluctuating quantities is unavailable.

A different approach to accounting for turbulent fluctuations is provided by Large Eddy Simulation (LES). This approach applies a spatial filter to the Navier-Stokes equations, with fluctuations larger than the filter width (typically the local cell size) being resolved, and fluctuations smaller than the filter width being treated with a sub-grid scale model, in a way analogous to a RANS model. LES allows for much more information to be gathered about fluctuating quantities than RANS models. This is because the fluctuations themselves (or at

least, the large ones) are directly resolved, allowing the user to carry out their own statistical analysis on them, in a way similar to how measurements in a flume would be analysed. In addition to this, treating large and small eddies differently means that LES can accurately model flows with large turbulence anisotropy and length scales. However, LES is significantly more computationally expensive than two-equation RANS models for two main reasons; firstly, LES has higher mesh requirements in boundary regions, and secondly, in order for converged statistical values of fluctuating quantities to be obtained, the model must be run for significantly more time steps.

The DDES (Delayed Detached Eddy Simulation) method used in this work is a hybrid turbulence model which endeavours to combine the advantages of LES in the wake region with RANS in near-wall areas in order to more accurately model the wake, whilst reducing computational expense to less than would be required for a pure LES model. This is achieved by recognising that, once averaging has been carried out (time averaging in the case of RANS, or spatial averaging for LES), information about the averaging method is lost, and both RANS and LES models become turbulence viscosity models. The DDES model compares the local turbulence length scale to the local cell size and uses this to decide to what extent the turbulence viscosity of the model should be modified from that obtained from a k-ω SST model (if at all). This results in a RANS model being applied in near wall areas, and LES-like behaviour being recovered in the wake region. Due to space requirements, the mathematics of the model will not be described in detail here, as the necessary information has been previously detailed in [47] and [54].

5 TURBINE PERFORMANCE, EXPERIMENTAL

Uncertainties were calculated using standard procedures[55, 56] and applying central limit theorem to quantities which have been obtained by averaging multiple samples of a population. These have been applied to measurements of flow velocity, turbulence intensity and turbine performance. Where error bars are displayed on charts, they represent confidence intervals of 95%. Where error bars are not displayed, they have either not been calculated (in the case of numerically integrated quantities such as Lt which would require very advanced methods to calculate and are beyond the scope of this work) or the calculated bounds of the 95% confidence intervals were within 1% of the reported value. In these cases, they have been omitted for clarity. Both CFD and experimental data are presented as curves, with crosses marking the positions where an experimental measurement was taken. If error bars are present, then the crosses may have been omitted, for clarity.

5.1 Flume results, lab scale turbine

Plots of C_P, C_T and thrust coefficient (C_θ) for the low turbulence, medium turbulence and high turbulence cases are shown in Figures 7a, b, c. Information regarding C_T was only available from the low-turbulence tests. The thrust data was determined via strain gauges on the stanchion at a clamping point above the waterline, so producing a bending moment from the force acting on the turbine and stanchion. It has therefore been included for indicative purposes but does not provide data for direct comparison with the CFD results, as these record the force on the turbine blades and hub only. Error bars on C_P and C_θ have been calculated using the procedure outlined in [45], with an assumed uncertainty in the mean velocity of ± 0.02 ms^{-1}, due to the use of the flume set-point rather than making simultaneous measurements of the flume velocity.

The curves of C_P and C_θ from the flume experiments show agreement, within the experimental uncertainties, between all three turbulence cases, demonstrating the same trends and similar magnitudes for all cases. As found in previous experimental work with this turbine, the position of maximum C_P was found to occur at $\lambda = 3.65$, with maximum torque occurring at $\lambda = 2.5$. Nonetheless, it appears that the medium-turbulence case has, in general, the lowest

C_P, the high-turbulence case the highest C_P, and the low-turbulence case between the two. This could be an indication of transition effects in the boundary layer of the turbine blades. As the Re at which the blade is operating is around the point of transition from laminar to turbulent flow. In general, it might be expected that an increase in turbulence, which will disrupt the flow over the turbine blade, will lead to a decrease in turbine performance, explaining the drop in performance from the low-turbulence case to the medium-turbulence case. However, due to the transitional nature of the boundary layer, it is possible that a separation bubble is being formed in these cases. With the large amount of turbulence in the high-turbulence case, it is unlikely that any separation bubble will survive due to the increase of energy in the boundary layer. If separation does not take place, then it is possible that, the turbine performance will actually increase in the high-turbulence case, reflecting the behaviour seen in Figure 7a.

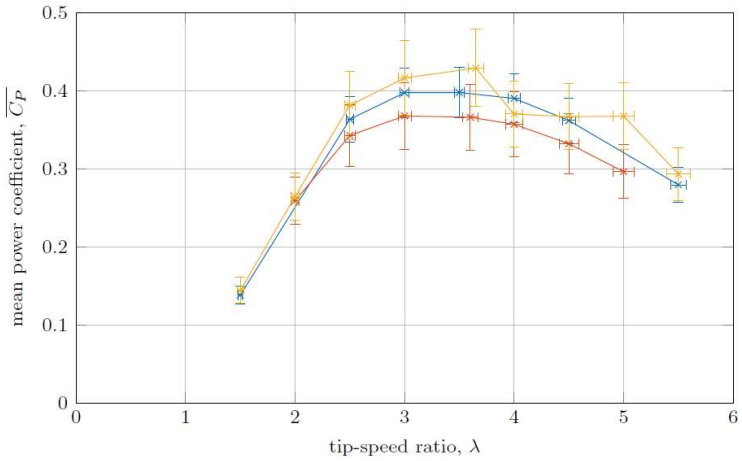

a

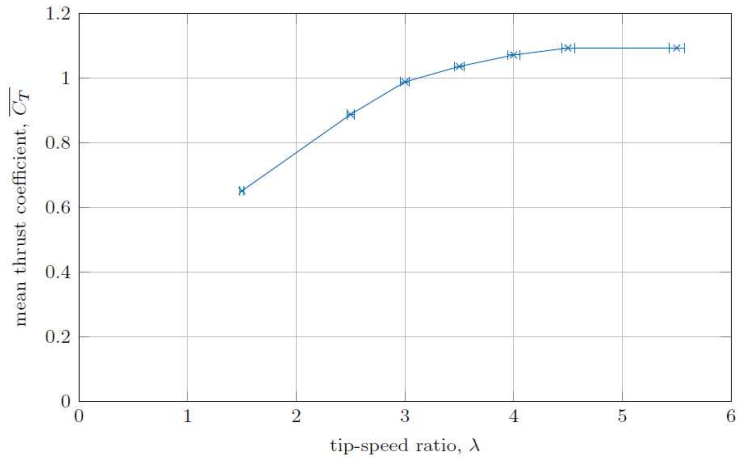

b

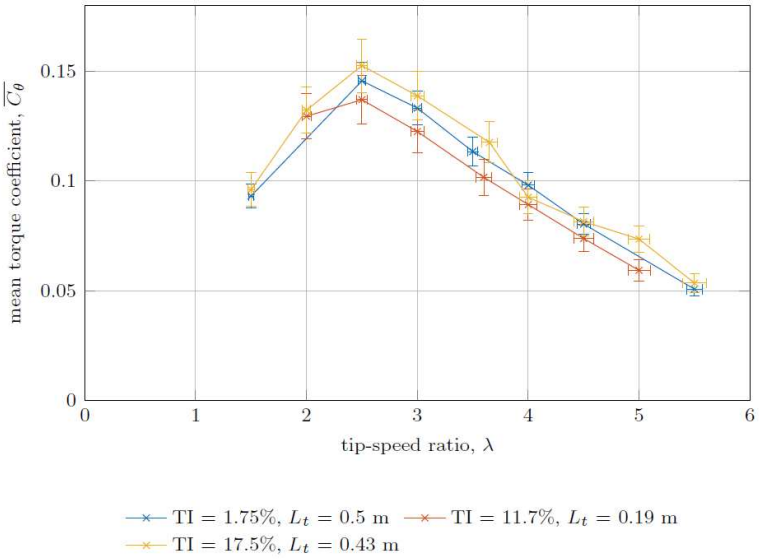

c

Figure 7 Flume results for **a)** C_P vs. λ. **b)** C_T vs. λ. C) C_θ vs. λ

5.2 Wake recovery

5.2.1 CFD results

Wake recovery will be primarily examined using centreline and volumetric averaged wake recovery curves, Figure 8. However, in order to fully understand some of the effects and impacts (particularly the impact of λ on the wake width), it is useful to present wake profiles for a typical case. Figures 9 present wake profiles for the low-turbulence CFD conditions. These profiles show that the shape of the wake is dependent on λ; with low λ, low-thrust cases leading to v-shaped wake profiles, and high λ, high-thrust cases leading to wake profiles which approximate a top-hat shape, the highest thrust cases leading to profiles with three minima.

5.2.2 Flume results

Results for the low TI, fine grid and coarse grid tests were analysed, with the centreline (Figure 8a), and volumetric averaged velocity recovery (Figure 8b).

Both of these figures show a clear trend - that higher TI is associated with faster wake recovery. This is expected, and follows trends found in previous experimental studies [13, 21]. Further to this, for the tests using grid-generated turbulence, the three λ values were used, and a trend is also apparent in all cases; λ = 2.5 shows the fastest overall recovery, with λ = 3.65 and λ = 4.5 showing similar rates of wake recovery. This would appear to then show a similar trend to that shown by the C_T curve (Figure 7b) with a larger difference between the thrust at λ = 2.5 and λ = 3.65, than between the λ = 3.65 and λ = 4.5 cases.

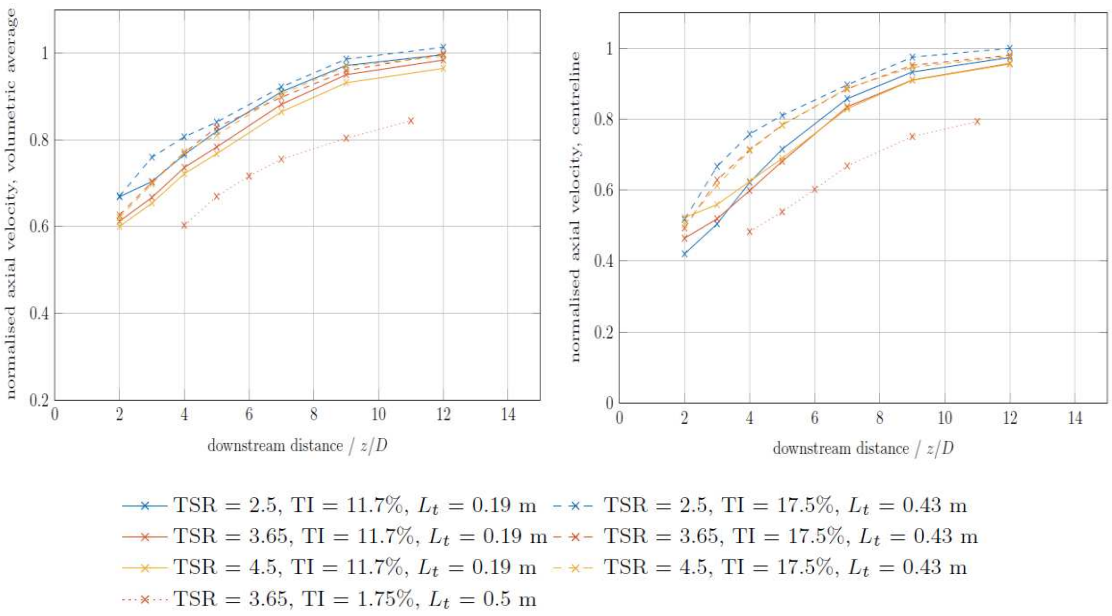

a) Centreline wake recovery. b) Volumetric averaged wake recovery

Figure 8: Wake recovery for flume measurements at all measured tip-speed ratios and turbulence intensities.

As expected for a wake recovering due to mixing with the free-stream, the centreline velocity (Figure 8a) is consistently lower than the volumetric average velocity (Figure 8b) until approximately z/D= 9 downstream of the turbine, where the normalised velocities becomes similar, regardless of which metric is used. This suggests that by this point the wake region has become homogeneous, and that the mixing layer has reached the centreline. One area of interest is the near wake (z/D ≤ 4) centreline recovery for the turbine downstream of the fine grid. In this region, the λ = 2.5 case is less recovered than the λ = 3.65 or 4.5 cases, in contrast to the overall trend for the rest of the wake. This suggests that the λ = 2.5 wake is demonstrating a large amount of inhomogeneity in this near wake region. This could be due to the fact that the blades in the λ = 2.5 case are producing less thrust, and therefore the influence of the nacelle is greater, leading to a lower velocity core when compared to the rest of the wake region. In addition to this, the λ = 2.5 case has the greatest rotational motion in the wake, which could be hindering wake mixing in this near-wake region. This trend is not apparent in the highest TI case, but this could be due to the greater level of turbulence leading to more mixing, making this effect less apparent. This is supported by CFD results presented in section 6.3.

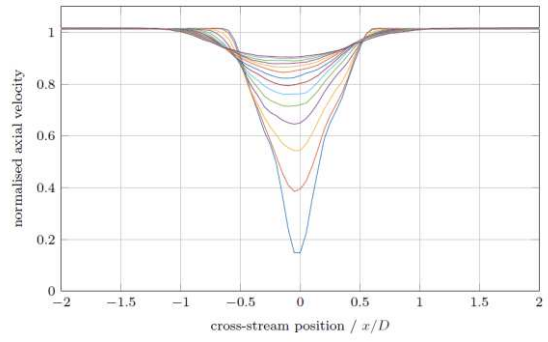

a: λ = 1.5.

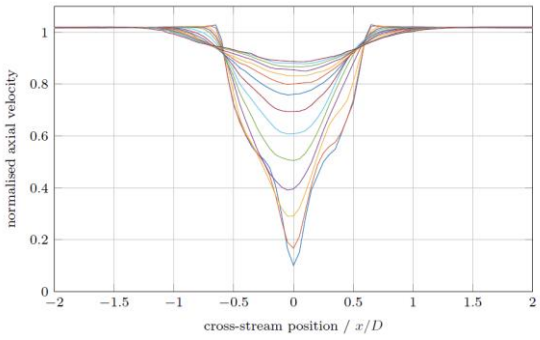

b: λ = 2.5.

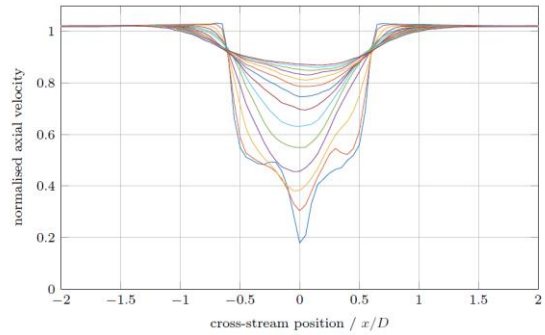

c: for λ = 3.0.

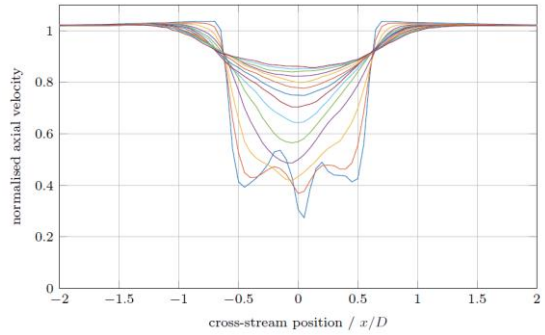

d: λ = 3.65.

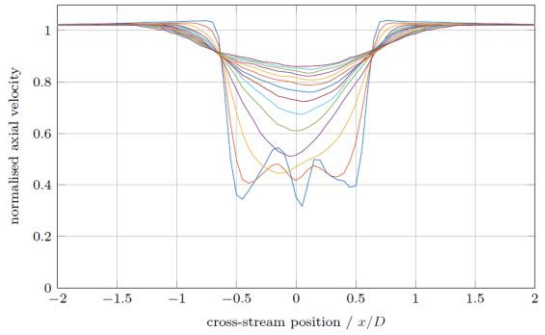

e: λ = 4.0.

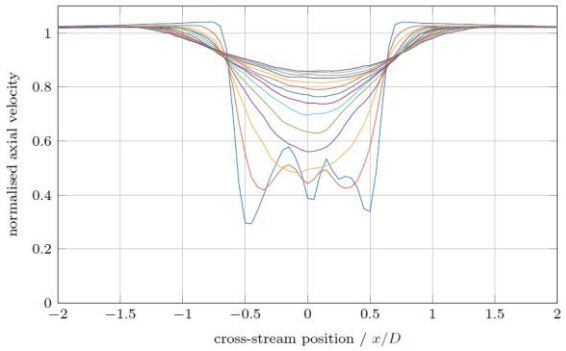

f: for λ = 4.5.

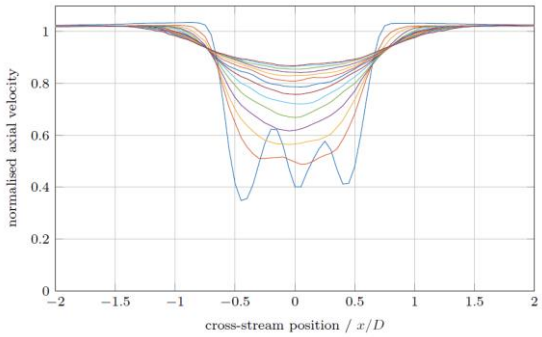

g: λ = 5.5.

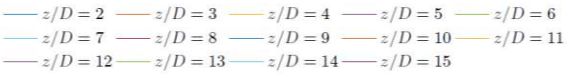

Figure 9: CFD wake profiles for the low-turbulence intensity

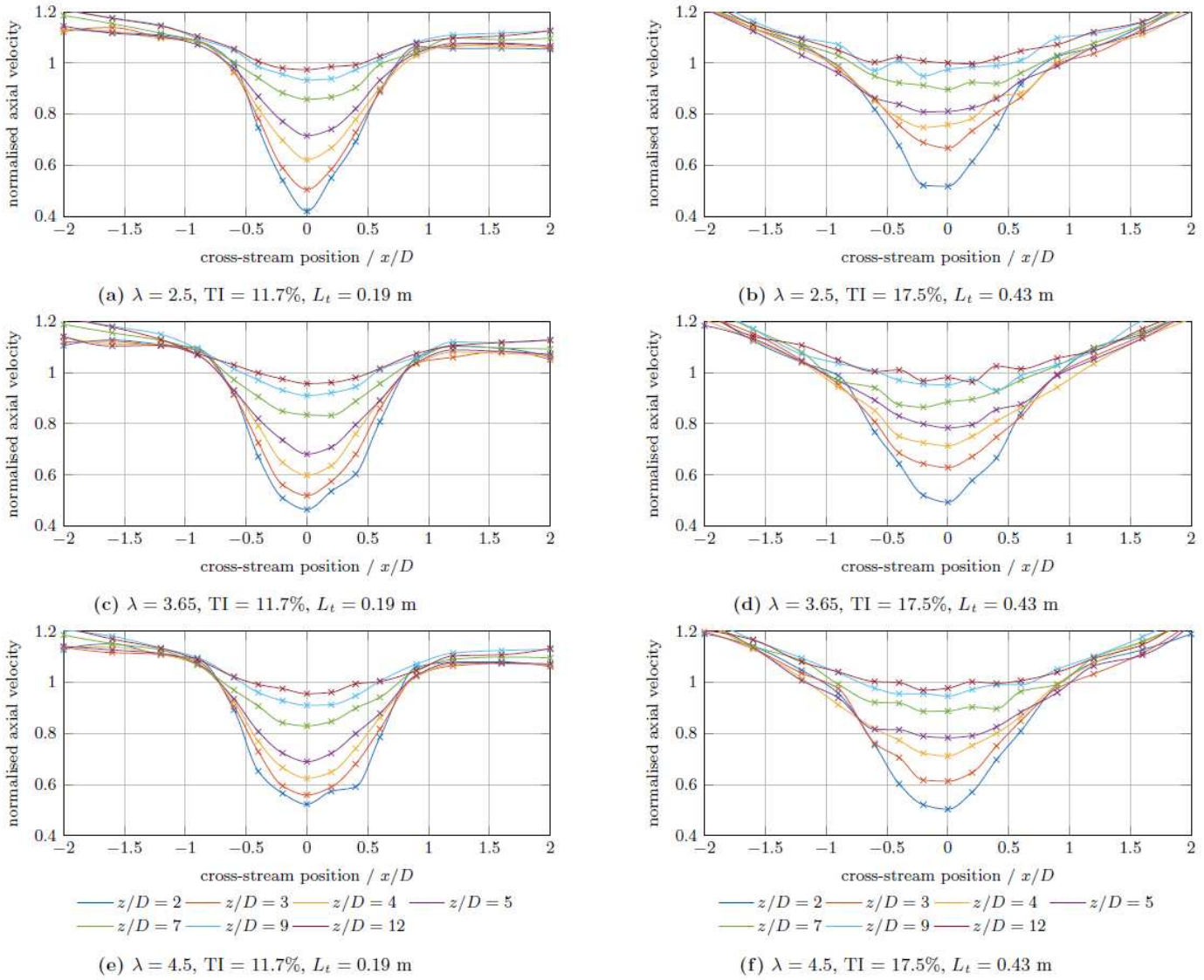

Figure 10: Wake profiles for the fine- (subfigures a, c, e) and coarse-grid (subfigures b, d, f) flume cases.

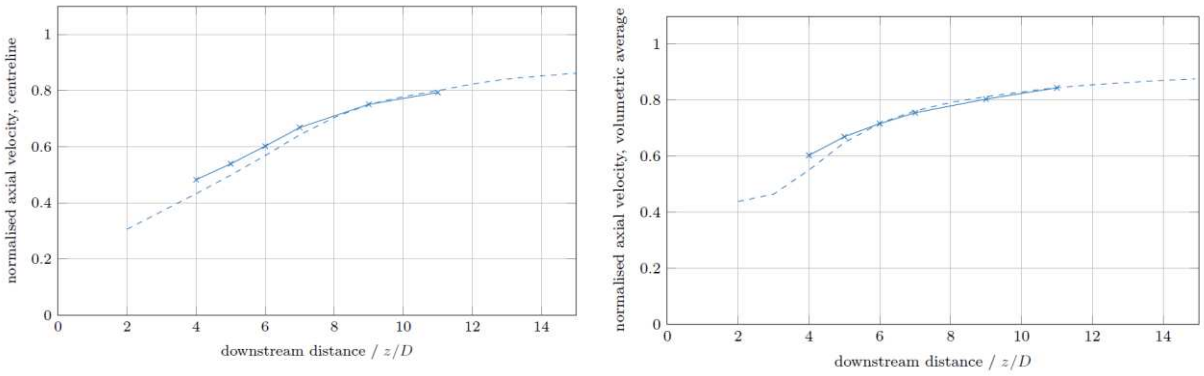

a: centreline wake recovery. **b:** volumetric wake recovery.

TSR = 3.65, TI = 1.75%, L_t = 0.5 m, flume
TSR = 3.65, TI = 0.96%, L_t = 0.8 m, CFD

Figure 11: Validation of low turbulence CFD

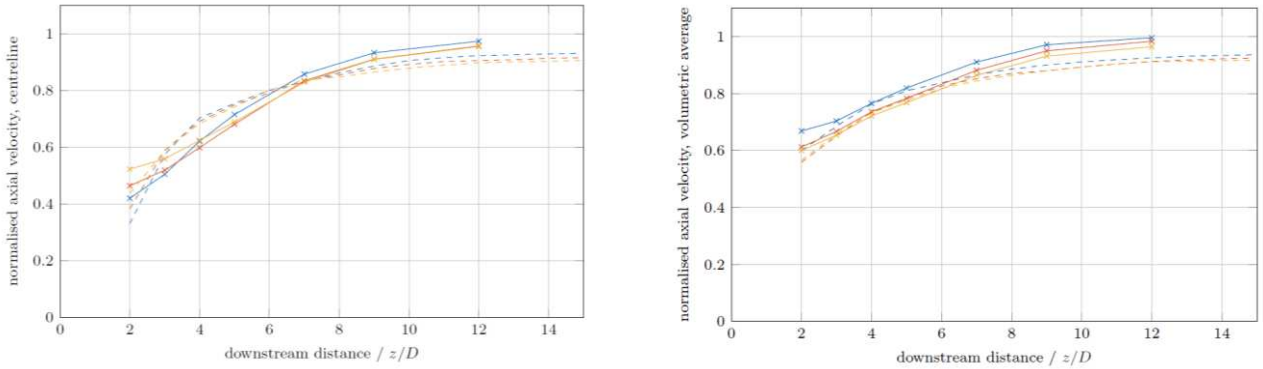

a: centreline. b:Volumetrically averaged

.

TSR = 2.5, TI = 11.7%, L_t = 0.19 m, flume
TSR = 3.65, TI = 11.7%, L_t = 0.19 m, flume
TSR = 4.5, TI = 11.7%, L_t = 0.19 m, flume
TSR = 2.5, TI = 11.4%, L_t = 0.19 m, CFD
TSR = 3.65, TI = 12.4%, L_t = 0.20 m, CFD
TSR = 4.5, TI = 12.4%, L_t = 0.20 m, CFD

Figure 12: Wake recovery validation using flume results with the fine grid

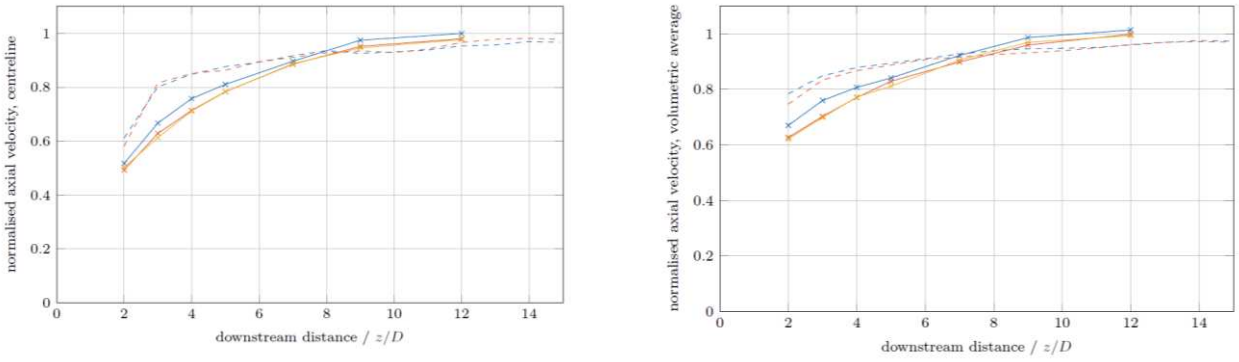

a: centreline b: volumetric averaged.

TSR = 2.5, TI = 17.5%, L_t = 0.43 m, flume
TSR = 3.65, TI = 17.5%, L_t = 0.43 m, flume
TSR = 4.5, TI = 17.5%, L_t = 0.43 m, flume
TSR = 2.5, TI = 16.6%, L_t = 0.41 m, CFD
TSR = 3.65, TI = 14.6%, L_t = 0.41 m, CFD

Figure 13: Wake recovery validation using flume results with the coarse grid.

5.2.2 Validation of CFD

Validation of the CFD for prediction of wake recovery is made for the low turbulence case by comparison of flume results to CFD along the centreline (Figure 11a) and for volumetric averaged wake recovery (Figure 11b). These both show good agreement in the region for which both CFD and flume data are available, with excellent agreement from z/D = 8 for the centreline recovery, and from z/D = 6 for the volumetric averaged recovery. It can be expected that the volumetric-averaged method will provide slightly better matching, as the combination of area-averaging as well as time-averaging makes this metric less sensitive to slight changes in the velocity distribution within the wake. The small discrepancies between flume and CFD results in the near-wake region can be explained by the fact that the flow field in this region is likely to be more complex and thus more difficult to accurately reproduce in a simulation. Mixing and recovery in the far wake is likely to be dominated by the outer shear layer of the wake, and therefore less dependent on the mesh directly around the turbine nacelle. This suggests that the DDES model has the ability to provide accurate predictions of the recovery of a turbine wake from at least the mid-wake region, in low-ambient turbulence conditions.

The validation plots for wake recovery for the tests behind the fine grid are presented in Figure 12a for the centreline wake, and Figure 12b for the volumetric averaged wake. As with the low TI case, agreement is better in the volumetric averaged wake, again probably due to the combination of both time and area-averaging. Agreement is generally good, although deteriorates beyond approximately z/D = 7, where the CFD under predicts the recovery by approximately 8%. The difference in recovery rates for the different λ values is well reproduced; in the volumetric-averaged recovery $\lambda = 2.5$ recovers faster than the other two cases, which show similar rates of recovery, with a tendency for the $\lambda = 3.65$ case to recover slightly faster than the $\lambda = 4.5$ case. Along the centreline, this trend of λ values showing faster recovery is reversed in the near wake region, but this is reflected in both the CFD and the flume results. At a downstream distance of $3 \leq z/D \leq 5$, the trend in wake recovery with λ reverts to that seen in the volumetric averaged wakes. Whilst the agreement between CFD and flume results behind the fine grid may not be quite as close as in the low-turbulence case, this is to be expected as it is unlikely that the CFD domain inlet will exactly reproduce the precise turbulence characteristics of the flume.

The validation plots for wake recovery for the testing campaign behind the coarse grid are presented in Figure 13a for the centreline wake, and Figure 13b for the volumetric averaged wake. Agreement in the mid- and far-wake is good, with a tendency for the CFD to slightly under-predict the recovery in the far wake, albeit only by around 5%. The CFD also tends to overpredict the recovery at distances of $z/D \leq 6$. As with the two previous flow conditions, the near-wake may be better reproduced with a finer mesh in the near-turbine region, but the discrepancies could also be explained by the high level of turbulence, and the CFD not exactly reproducing the turbulence characteristics of the grid-generated turbulence.

6 IMPACT OF TURBULENCE ON WAKE RECOVERY

6.1 Turbulence intensity

The impact of ambient TI on wake recovery is examined using the results in Figures 8 for flume centreline and volumetric averaged velocities. In addition, four selected CFD cases were compared which have similar turbulence conditions to each other except in respect of TI. The flume results with higher TI exhibiting more rapid wake recovery for both centreline and volumetric averaged results (Figures 8). For the volumetric averaged wake recovery curves, the wakes produced behind the fine grid and those behind the coarse grid still show only a slight difference, suggesting that there may be an upper limit beyond which an increase in TI has little further effect on wake recovery.

The CFD results are in general agreement with the flume results, with the figures for centreline and volumetric averaged wake showing very similar behaviour (Figures 11 - 13). Here it can also be seen that a higher TI promotes faster wake recovery, with the two cases of greatest TI showing similar results from the mid-wake onwards. These results follow trends seen in previous experimental work [13, 21], with the consensus being that higher ambient turbulence promotes mixing and transfer of momentum across the wake shear layer, increasing the velocity of the wake region, and promoting wake recovery.

6.2 Turbulence length scale

The impact of turbulence length scale on wake recovery was explored using three selected CFD runs. The results are presented in Figures 14 for the centreline and volumetric averaged wake recovery, respectively. In both cases the medium L_t case (0.78 m) initially shows a fast recovery to approximately 90% of the free-stream velocity, after which very little further recovery takes place. From z/D = 8 the case with the largest L_t (1.5 m) shows the greatest recovery. The cases with the smaller L_t sizes (0.45 and 0.78 m), showing a reduced rate of recovery. This suggests that L_t may have an impact in the far wake as the case presented with the largest L_t also has the lowest TI, which would tend to reverse the order seen in the far wake.

In the near- to mid-wake (z/D< 7), the shortest L_t has a faster centreline recovery than the largest L_t, however, this trend is reversed for the volumetric averaged recovery. This could indicate that the short length scales increase mixing within the wake region (and therefore promote centreline wake recovery) in the near wake, with the larger length scales dominating the mixing between the wake and the free-stream, which ends up dominating overall wake recovery. The effect of momentum transfer across the outer shear-layer of the wake will first be apparent in the volumetric-averaged recovery, with this trend reaching the centreline later. This could indicate that larger length scales lead to slower initial, but faster overall wake recovery. Nonetheless, the behaviour is complex and is difficult to completely isolate the effects of L_t and TI. In addition, this study only compares three different length scales, making non-linear effects difficult to identify.

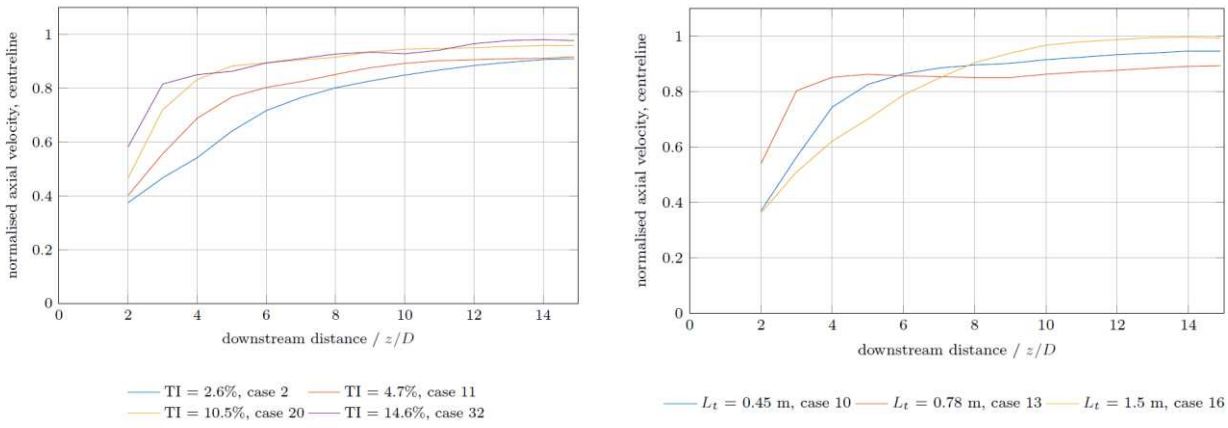

a: ambient turbulence intensity

b: ambient turbulence length scale

Figure 14: Impact of a) ambient turbulence intensity and b) length scale on centreline wake recovery, CFD cases.

6.3 Impact of tip-speed ratio on wake recovery

The impact of turbine operating condition on wake recovery can be examined using Figures 15 which examines the impact on the volumetric averaged wake recovery. The example shown is from CFD in the low-turbulence case at λ = 3.65 (Appendix: Table A.1, runs 34 - 40). Comparison of the two metrics allows assertions to be made about the homogeneity of the

velocity distribution in the wake region. If the trends are similar, this suggests a more homogeneous wake, where they are not, which indicates that the velocity has a strong dependence on radial position.

The centreline velocity recovery shows a clear trend with tip-speed ratio. The higher the tip-speed ratio, the greater the initial wake recovery. Nonetheless, beyond approximately z/D = 10, the tip-speed ratio seems to have little impact on the centreline wake recovery. This appears to follow the trend of the thrust curve of the turbine, with higher thrust cases showing a higher centreline recovery. This might appear counter intuitive, as a turbine with higher thrust will be presenting more resistance to the flow, causing flow to divert around the rotor swept area. However, most of the thrust is produced by the outer portion of the blades, causing flow to be diverted not only outside and around the swept area, but also inwards towards the blade roots and nacelle. This increases the velocity towards the centreline, encouraging centreline wake recovery. This effect can be seen by comparing Figures 9a-g, showing the wake velocity profiles for tip-speed ratios of $1.5 \leq \lambda \leq 5.5$, at downstream positions from $2 \leq z/D \leq 15$. Low-thrust, low tip-speed ratios have profiles which are v-shaped, but as the tip-speed ratio and thrust increases, the shapes of the wake profiles become more like an inverted top-hat, with the highest-thrust cases exhibiting 3-dips in the nearest profiles. The peaks between these dips indicate flow being diverted inwards, towards the turbine nacelle, leading to the wake recovery curves seen in Figures 15. This trend in the shapes of wake profiles with tip-speed ratio agrees with the wake profiles measured in the flume, presented in Figure 10. The triple-dip profile at z/D = 2 is not seen in these profiles from the flume; however, given the much higher levels of turbulence and increased recovery it is to be expected that this level of detail in the profiles may not be seen. Indeed, the change in profile shape becomes less clear between the fine grid (Figures 10a, 10c and 10e) and coarse grid case (Figures 10b, 10d and 10f). An exception to the overall trend is the $\lambda = 1.5$ case. In the very near wake, this curve appears to approximately fit the trend for tip-speed ratio, but thereafter recovers at a much greater rate than any of the other curves, such that, by z/D = 5, it has shown the most recovery - a trend which continues further downstream. Frost provided detailed characteristics of the turbine and showed that at a tip-speed ratio of $\lambda = 1.5$ the turbine is operating in the stall-region [45]. A stalled blade can be expected to produce increased turbulence in the near-wake region than an un-stalled blade (due to flow separation over the blades themselves), contributing to more mixing in this region, whilst at the same time producing less thrust. Given this, it might be expected that the influence of the turbine nacelle might be greater in the very near wake for the $\lambda = 1.5$ case than for other tip-speed ratios, but that the effect of increased blade turbulence causes rapid mixing and consequently rapid wake recovery.

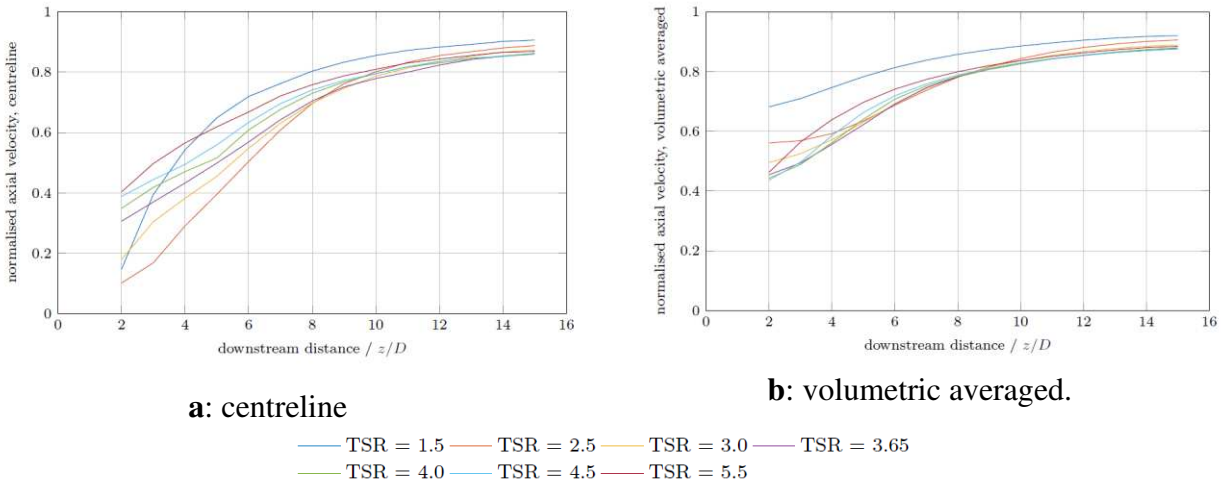

a: centreline

b: volumetric averaged.

Figure 15: Impact of TSR on wake recovery for low ambient turbulence condition.

The volumetric-averaged wake recovery curves presented in Figure 15b show a slightly different trend, whereby the λ values with the highest C_P tend to show the largest deficit in the near wake. This makes sense as the high C_P cases will extract more energy from the flow, by means of reducing flow velocity. Nonetheless, this effect is only apparent in the near-wake; beyond z/D ~ 4, all cases except for λ = 1.5 and λ = 5.5 are virtually indistinguishable from each other, with the λ = 5.5 case merging at ~ z/D = 8.

As with the centreline wake recovery, the λ = 1.5 case appears to be an outlier, showing greater wake recovery than any other case. This case has the lowest power and thrust coefficients of all of the cases in the figure, meaning that the turbine neither extracts much energy from the flow, nor provides great resistance to it. This leads to flow passing through the turbine swept area without being slowed down, and hence the wake is well recovered. A comparison of Figures 15 shows that the λ = 1.5 case is highly inhomogeneous in the near wake, with a low velocity centreline surrounded by an otherwise well recovered wake.

For array designers, the most important conclusion to be drawn from Figure 15b is that (with the exception of the stalled case of λ = 1.5) beyond z/D = 8, tip-speed ratio has little impact on the volumetric-averaged wake recovery. This means that even in the case where a turbine uses an over-speed regime to maintain rated power, there will be no impact on the longitudinal spacing (assuming the turbines are separated by at least 8D).

7 WAKE WIDTH

7.1 Flume results

Flume results for the wake width using the fixed-threshold, full-width half-minimum and maximum-shear methods are shown in Figures 16. Examining Figure 16a for the fixed-threshold method, it can be seen that, for all cases, the wake at z/D= 2 is between 1-1.5D in width, with the width decreasing as the wake develops. This is to be expected as the fixed-threshold wake method is intrinsically linked to the wake recovery.

Recalling that the fixed-threshold method measures the width of the wake region which is less than 90% recovered, it is clear that, as the wake recovers, the region which is less than 90% recovered will tend to decrease. Assuming that recovery is symmetrical about the centreline, when the centreline velocity recovery reaches 90% of the free-stream, the wake width using this metric will become zero. This connection between wake recovery and fixed-threshold wake width explains the differences between the low-turbulence case (TI = 1.75%) and the cases behind the coarse and fine grids. The centreline wake recovery (Figure 8a) shows that both grid-generated turbulence cases demonstrate 90% wake recovery in the region $7 \leq z/D \leq 9$, whereas the low-turbulence case has only achieved approximately 80% recovery by z/D = 11 downstream, where the measurements ended. This lack of mixing and recovery in the low-turbulence case explains why the wake persists for longer, leading to a wake that retains its width for longer (Figures 16a 16b). It appears that a higher ambient TI leads to a slightly greater wake width in the near wake region, but the coarse and fine grid cases (TI = 11.7% and 17.5% respectively) show little difference from one another beyond z/D= 6. In addition to this, for the cases of grid-generated turbulence, there appears to be a dependence of wake width on tip-speed ratio, with greater λ leading to slightly wider wakes throughout their entire length. This is thought to be due to increased thrust on the turbines at the higher λ causing more flow to divert sideways and around the turbine, increasing the wake width.

A greater thrust on the turbine will tend to divert the oncoming flow outside and around the turbine swept area, causing a wider wake. The wake width results following the full-width half-minimum method for all flume cases are presented in Figure 16b. The shapes of the curves are slightly different to those seen in Figure 16a as the two metrics are affected in different ways by the shapes of the velocity profiles, however, the major trends from the fixed-threshold method are also apparent in the full-width half-minimum method. The same dependence of

wake width on tip-speed ratio is apparent, with higher tip-speed ratios (and therefore higher thrust) leading to wider wakes. In addition to this, as before, the width of the wake in the low-turbulence case seems to persist for much further downstream than in the higher-turbulence cases. It is thought that this is due to less mixing being present, allowing the wake to maintain its shape further downstream. Again, as in the fixed-threshold case, the wake width in the high-turbulence case is initially highest of all, perhaps due to increased mixing broadening the shear layer between the wake and the free-stream. As the wake develops downstream, the high-turbulence case seems to narrow at a faster rate than the other cases, possibly due to increased mixing.

Wake width results for the flume cases following the maximum shear approach are presented in Figure 16c. It could be suggested that the case with the highest turbulence tends to produce a wider wake, but beyond this, no clear trends are visible. The much longer wake for the low TI case is due to the unusually small amount of mixing taking place, and whilst interesting for gaining insights into the mechanics of wake mixing, is of little relevance to turbines in practical marine locations.

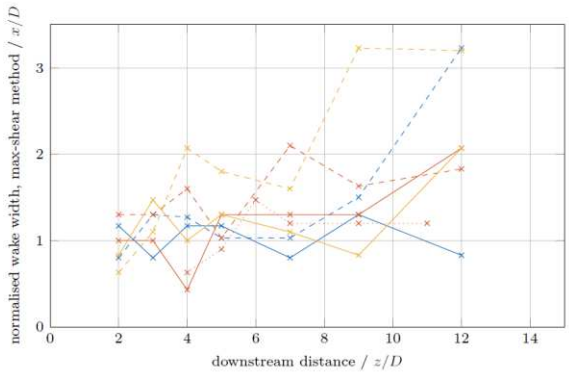

a: fixed-threshold method.

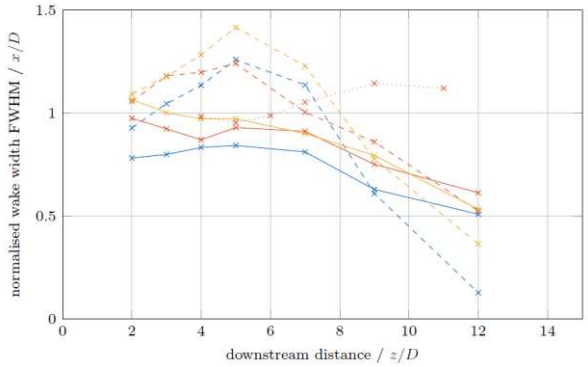

b: full-width half-minimum method.

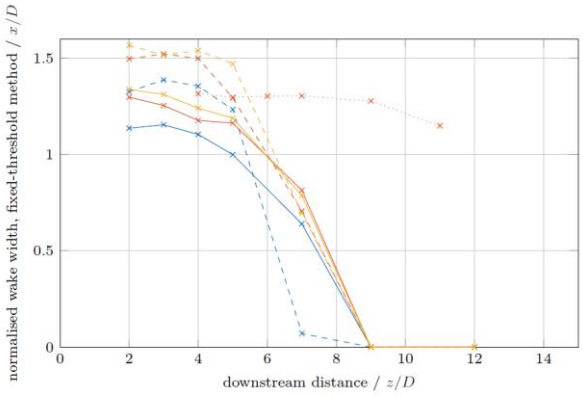

c: maximum-shear method

Figure 16: Flume wake width

7.2 CFD

Validation of the CFD against the low-turbulence flume tests can be seen for the fixed threshold method, full-width half-minimum method and maximum-shear method in Figures 17. Validation of the CFD using the fixed-threshold method in Figure 17a, shows good agreement between the CFD and the flume results, with both showing a slight narrowing of the wake as it develops downstream, and only a slight under-prediction of wake width by the CFD. A slight under-prediction of wake width by the CFD is also apparent in Figure 17b, which compares

CFD and flume results using the full-width half-minimum method. As with the fixed-threshold method, there is good agreement with the trend of wake development, this time with both methods showing a slight widening of the wake with downstream distance. Agreement between the CFD and flume results using the maximum-shear method (Figure 17c) is less clear, although as mentioned in the discussion of Figure 16c, and further discussed in section 7.3, results for the maximum-shear method suffer from convergence difficulties. Nonetheless, both CFD and flume results indicate a slight widening for the wake with increasing downstream distance, and CFD and flume results show a wake width of the same order of magnitude. Agreement is not as good as with the fixed-threshold and full-width half-minimum methods.

The flume and CFD results using the fixed-threshold method found that both sets of results follow the same overall trends; starting with a near-wake width of 1.1 - 1.5D and staying almost constant for 3 – 5D downstream, before narrowing. The CFD results show the same trends with λ as the flume results. The CFD does though tend to under-predict the rate of wake narrowing, with changes in the CFD predicted wake occurring 2 - 4D further downstream than that seen in the flume.

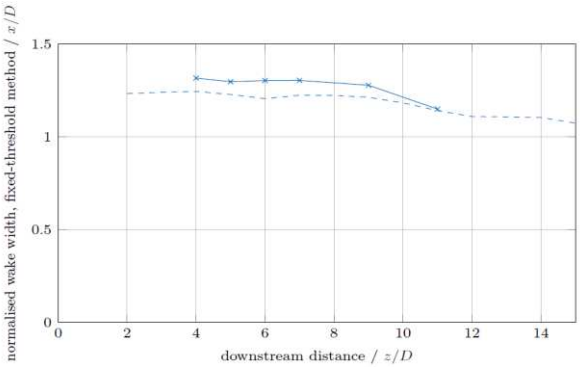

a fixed-threshold method.

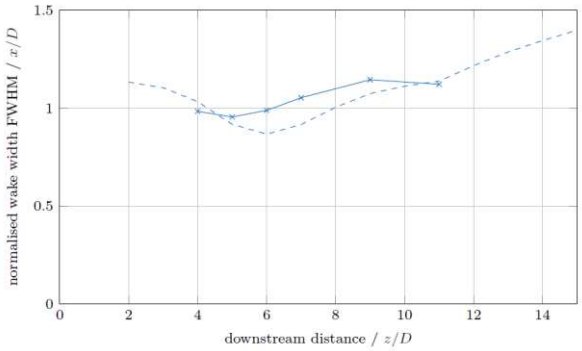

b the full-width half-minimum method.

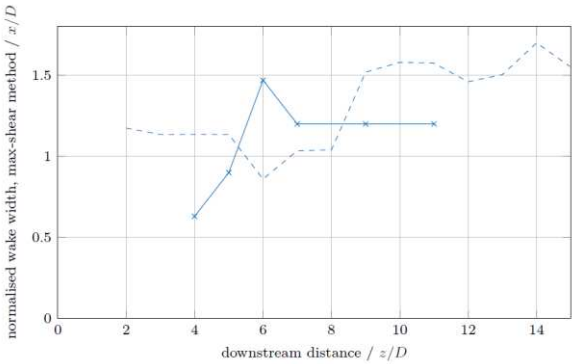

c maximum-shear method

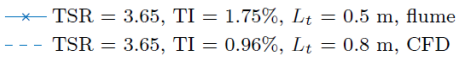

Figure 17c Validation of low-turbulence wake width

The flume and CFD results using the full-width half-minimum method found that initially there is close agreement between the flume and CFD results in the near-wake, but that from this point the results diverge, with the CFD results trending slightly wider than the flume results. The trend with λ seen in the flume results is reproduced in the CFD results. Using the full-width half-minimum method, the increase in wake width with downstream distance might be expected, as the method gives an indication of the width of the region being in some way affected by the wake, and this will tend to get wider as the wake mixes with the free-stream. The reason for the flume results showing a narrowing with downstream distance is not entirely clear, but if the wake profiles in Figure 10 are examined, then it can be seen that, outside of the wake region, the profiles indicate an increased axial velocity, and show a slight asymmetry and inhomogeneity in the flume outside of the immediate wake region. This will affect the shapes

of the profiles as well as making the choice of a reference velocity for normalisation and calculation of deficit less clear, therefore affecting the width calculated using the full-width half-minimum method. For the flume results the axial velocity used for normalisation and deficit calculation is that which appears in Table 1, following measurement of the centreline flow conditions in the flume at the point at which the turbine was placed. CFD results were normalised and wake deficits calculated using the measured values for axial velocity .

For the coarse grid wake widths calculated using the fixed-threshold method again showed good agreement between the CFD and flume results. All wakes show an initial width of between 1 - 1.5D, which remains nearly constant until $5 \leq z/D \leq 7$, at which point they narrow rapidly. For both flume and CFD results the initial wake width narrowing, and the rate of narrowing are all well matched, as is the trend of an increasing wake width with λ.

Agreement between CFD and flume results for the fixed-threshold method appears to be slightly better in the case of the coarse grid than for the fine grid. This is thought to be due to the increase in mixing due to the higher TI conditions, and the inherent link between this width metric and wake recovery. The turbulence in the coarse grid cases increases the mixing and consequently the wake recovers very rapidly, with the 90% threshold being very quickly achieved. This means that the wake widths very quickly drop to zero following this metric. A more gradual wake recovery means there is less rapid mixing in the fine grid cases.

As with the full-width half-minimum results for the fine grid case, the flume and CFD results for the coarse grid show good agreement in the near-wake region, before diverging, with the flume results indicating a narrowing of the wake, whilst the CFD results indicate a widening of the wake Again, examination of Figure 10 indicates that there is some asymmetry and inhomogeneity in the flume (due to the presence of the grid), and this will tend to distort the shape of the profiles, and affect the width calculated using the full-width half-minimum method.

Agreement, for all cases of turbulence and operating conditions, is only reasonable at best when using the maximum-shear method. There is a general indication that higher-thrust cases yield a wider wake as expected, however, the lack of convergence using this method means that there is no clear trend in the far wake.

7.3 Evaluation of different width metrics

Three different wake width measurement metrics have been applied in this paper:

1. the fixed-threshold method,
2. the full-width half-minimum method, and
3. the maximum-shear method.

As the wake width can be difficult to define, these three metrics were applied as they each provide a slightly different insight into the wake behaviour. The fixed-threshold method yields the width of the region strongly impacted by the wake. In this work, the threshold was chosen to be 90% wake recovery, which in conditions of high ambient TI meant that the wake width reduces to zero within the region studied (i.e. $z/D \leq 15$). By contrast, the full-width half-minimum method applies a threshold, but calculates that threshold based on the maximum deficit at that downstream distance. Consequently, this method provides a value for wake width which is related to the total width of the region impacted by the wake (i.e. the region where the velocity has been changed due to the presence of the turbine). It may be seen as a measure of the extent to which the wake has extended out into the flow region surrounding that directly downstream of the turbine. Applying both the fixed-threshold and full-width half-minimum methods allows an assessment to be made of how the wake is developing/recovering; for example, it might be found that the full-width half-minimum method indicates a widening of the wake, whilst the fixed-threshold method indicates a narrowing of the wake. This would

indicate that the width of the region affected at all by the wake is increasing, but that this impact grows weaker as downstream distance increases.

The maximum-shear method does not try to define the wake width in terms of regions of greater or lesser impact, but rather uses the velocity shear to attempt to define the mid-point between the wake region and the free-stream. It is useful in as much as it defines a point within the flow, but as the wake develops and width of the shear layer between the wake and free-stream increases, the shapes of the wake profiles also change, and this definition of a point between the wake and free-stream regions becomes less useful as a comparison metric between wake profiles of different shapes. This is, in part, because this method as applied in this paper only accounts for the position of the point of maximum shear but pays no regard to the strength of the shear. In addition, when applying these three methods it was found that they respond differently to wake profiles of different shapes. In particular, the maximum shear method showed itself to be particularly sensitive to slight changes in the mean flow-field when the wake profiles were approximately v-shaped. The three methods have been applied to the low turbulence CFD case, $\lambda = 3.65$. Each of the metrics has been applied to the same velocity data, so any difference in the rates of convergence are due to sensitivity inherent in the metrics themselves, rather than a lack of convergence in the velocity data. For reference, wake velocity profiles for this run can be seen in Figure 9. The reader will notice some slight asymmetry in the wake. This is thought to be due to the asymmetry in the experimental setup (and CFD). The walls and floor of the flume were modelled as no-slip boundaries, whereas the upper domain boundary was set to a zero-shear condition.

As the wake develops with downstream distance, the shape of the velocity profiles changes from one with very steep sides (shaped approximately like an inverted top-hat) to profiles which are v-shaped, with an almost linear change in velocity with cross-stream position, and therefore an almost uniform velocity shear from near the centre to the very edge of the wake. This transition is a gradual one, but by approximately $z/D = 6$, the profiles have become distinctly v-shaped. For the inverted top-hat profiles, their steep-sides mean that the point of maximum-shear is located within a relatively small cross-stream extent. Any small changes in the mean flow field have little impact on the cross-stream position of the point of maximum-shear, and therefore the value of wake width in this region converges quickly. In contrast to this, for v-shaped wake profiles the almost linear change in velocity with cross-stream position means that there is a large cross-stream extent with an almost identical amount of velocity shear, the value of which is approximately the same as that of the maximum-shear. The result of this is that any small changes to the mean velocity field (and therefore the wake profiles) can cause the position of maximum-shear to move from nearly the centreline to the very edge of the wake, despite there being no significant change to the wake profile itself. This means that the wake width based on the point of maximum-shear can vary greatly, and the metric is very sensitive to slight changes in the velocity profiles. A schematic comparing the three different metrics is presented in Figure 18. This comparison varies depending on the precise tip-speed ratio and inlet flow conditions; the representation here is based on the behaviour for tip-speed ratios around the point of maximum C_P for low turbulence conditions and is intended to show the general behaviour of the metrics, but is not intended to be to-scale. All three metrics initially have a similar width, slightly larger than the turbine diameter. The width measured using the fixed-threshold method tends to decrease as mixing takes place and the wake recovers. In contrast to this, the full-width half-minimum method initially shows a decrease in width as the wake velocity profile changes from an inverted top-hat shape to a v-shape, before showing a steady increase as the mixing region between the wake and the free-stream spreads outwards. A similar trend occurs with the maximum-shear method, which initially exhibits a nearly constant width (due to the inverted top-hat shape of the wake velocity profiles). As the wake profiles become more v-shaped, the maximum-shear method starts to demonstrate convergence issues, and only

a general trend of increasing width can be identified. This is represented in this schematic by the movement and fading of the line representing this metric. Comparing Figure 18 to Figure 1, it can be seen that the fixed-threshold method behaves in a similar way to the inner edge of the shear layer (between the shear layer itself and the wake core), whereas the full-width half-minimum method comes closer to representing the general expansion of the wake into the free-stream region.

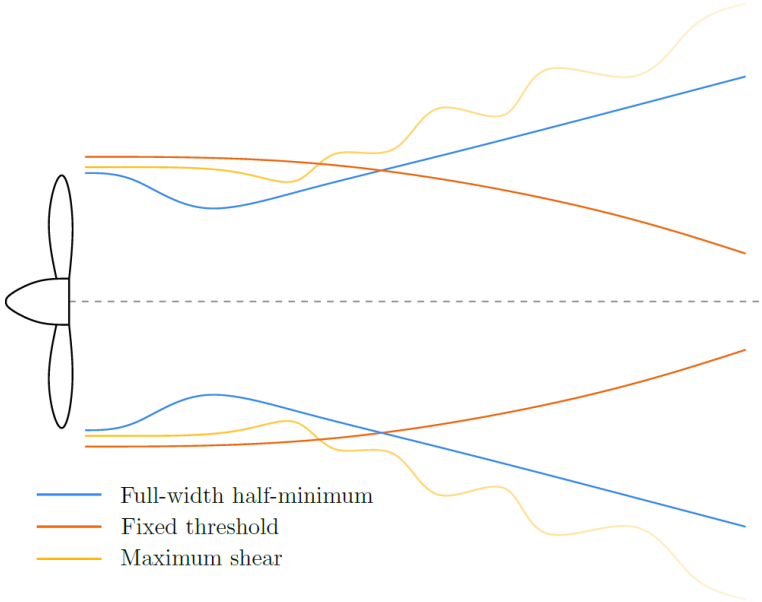

Figure 18 Schematic (not to scale) comparing the general behaviour of the three different wake measurement metrics.

The maximum-shear method always gives a wake `edge' within the shear layer, but as the shear layer increases in thickness and the wake velocity profiles become v-shaped, this could be anywhere from the boundary between the shear layer and core region to the boundary between the shear layer and free-stream, which leads to this metric's poor convergence. The maximum-shear method only gives reliably converged results in the near wake, where the shear layer between wake core and free-stream is thin and distinct.

Given that the maximum-shear method shows convergence difficulties for v-shaped profiles which appear both in CFD results and the fact that the fixed-threshold and full-width half-minimum methods provide information with direct applicability to array designers, it is suggested that the maximum-shear method is of limited value in the discussion of wake width.

7.4 Impact of turbulence on wake width

7.4.1 Turbulence intensity

The impact of TI on wake width is explored using the fixed threshold, full-width half-minimum and maximum-shear methods.

The fixed-threshold metric shows that, regardless of ambient TI, all wakes initially have very similar widths. These start to diverge from approximately z/D= 5 downstream, with the cases with higher TI showing a more rapid narrowing than those with lower TI. This is due to the increased levels of mixing encouraged by the higher turbulence intensities. The fixed-threshold method provides an indication of the width of the region strongly affected by the presence of the turbine; more mixing and faster wake recovery means that the region of the highest velocity deficit will reduce more rapidly, narrowing the wake by this metric.

The full-width half-minimum metric shows a general steady increase in wake width for all TI cases, whilst showing that the higher TI cases yield a wider wake. This can again be explained by the increased levels of mixing from the higher TI ambient flow. The full-width

half-minimum method gives an indication of the width of the region impacted at all by the wake; increased mixing between the wake and free-stream leads to a faster transfer of momentum to the wake region from the free-stream (leading to faster wake recovery), but also means that the effect of the velocity deficit in the wake region will be moved further and faster into the free-stream. This leads to a greater width being affected to some extent by the wake in the higher TI cases, whilst simultaneously reducing the width of the region strongly affected by the wake.

The maximum-shear method also indicates a dependence of wake width on TI, with the higher turbulence cases there is a trend to increasing wake width. This gives some information about the shape of the wake recovery profiles and suggests that they become flatter with slightly steeper sides as TI increases. Another way to see this is that the wakes become more homogeneous with increased TI, reflected in the increased centreline velocity recovery (Figure 14a). As discussed, choosing to define the point of maximum-shear in the wake as the `edge' of the wake, has less meaning than the fixed-threshold and full-width half-minimum methods, which either give the region strongly affected by the wake, or the region affected to some extent, and, whilst it is interesting to see a dependence of the maximum-shear method on TI, it does not give any real insight for array designers.

Overall, it can be said that an increase in ambient TI has an impact on the width of the wake of a tidal stream turbine. The increase in mixing associated with the increase in TI means that the width of the region of highest velocity deficit reduces more rapidly, whilst at the same time, the overall wake width increases (albeit with its impact weakened). This result will be important for array designers and suggests that, combined with the results for velocity recovery, arrays in areas of higher ambient TI may benefit from a reduced longitudinal spacing, and increased lateral spacing. In effect, higher TIs tend to shorten and widen wakes.

7.4.2 Turbulence length scale

The impact of turbulence length scale on wake width is examined using the fixed threshold, full-width half-minimum and maximum-shear methods. The fixed threshold method shows that the width in the case with medium L_t (0.78 m) remains fairly constant, whereas that with the shortest L_t (0.45 m) shows the widest initial width with rapid narrowing.

The case with the longest L_t (1.5 m) shows a similar trend to that of the shortest L_t, albeit with a less rapid narrowing. There is, however, no clear overall trend of wake width with length scale using this method. The full-width half-minimum method resulted in the mid-wake region ($3 \leq z/D \leq 11$) with the shortest L_t having the widest wake, whilst the longest L_t shows the narrowest. From $z/D \sim 11$, the longest length scale, then results in the widest width. This could suggest that the largest turbulence length scales demonstrate less initial mixing (and therefore the narrow wake in the mid-wake region), but a more thorough mixing in the far wake region. Similar behaviour is also found when the maximum-shear method is applied.

Overall, there is no clear trend of impact of L_t on wake width, regardless of which metric is used. However, only three different length scales have been compared here, and it has not been possible to completely isolate the effects of TI and length scale. It might also be the case that turbulent length scales smaller or larger than those used here could have a different impact and would be worthy of further investigation to establish any possible impact.

7.5 Impact of tip-speed ratio on wake width

Regardless of which metric is used, there is a clear trend in the data that an increase in λ results in a wider wake. This trend is clearest when the fixed-threshold method is used. Here, all wakes maintain their initial width or widen slightly, before tending to narrow with downstream distance. All the wakes show the same general trends, but with the lowest thrust cases in general being the narrowest. The differences in width are most apparent for the low λ

values, whilst the higher λ values are more closely grouped together. This corresponds well to the thrust curve. The same overall trend was found in wake widths calculated using the full-width half-minimum method. As with the fixed-threshold method, the cases where the turbine is operating at a higher thrust demonstrate a greater wake width. However, with the full-width half minimum method, the overall trend is that the wake width steadily increases with downstream distance. This difference, when compared to the fixed-threshold method, is due to firstly, the way that the two methods respond to wake profiles of different shapes, and secondly, as the full-width half-minimum method is a measure of the width of the region impact to some extent by the wake, this can be expected to increase as the wake spreads out downstream, even if its strength diminishes. The cases closest to peak power, with $3.0 \leq \lambda \leq 4.5$ initially show a reduction in wake width until z/D ~ 6 downstream of the rotor, after which they steadily increase in width. $\lambda \geq 3.65$ all show the same initial width, with the $\lambda = 3.0$ case showing a similar initial width as well. All of these cases show a profile with very steep sides, similar to an inverted `top-hat' shape, in the near wake. These steep sides are only slightly wider than the turbine and are in the same position regardless of the velocity deficit in this region. Applying the full-width half-minimum method to an inverted top-hat shape will give an almost identical result for wake width, regardless of the maximum velocity deficit. This leads to the near-wake width of each of these cases being nearly identical. In contrast, the low thrust cases with tip-speed ratios of $\lambda = 1.5$ and 2.5 do not show these inverted top-hat profiles but show v-shaped profiles instead. As these v-shaped velocity profiles develop downstream, they reduce in depth and become proportionally wider, which is reflected in the steady increase in width measured using the full-width half minimum method. For the cases where the initial profile is that of an inverse top-hat, as the wake develops and mixes with the free-stream this inverse top-hat first becomes U-shaped, then v-shaped (leading to the apparent decrease in wake width), from which point the profiles reduce in depth and become proportionally wider, matching the trend shown with the low-thrust cases. These profiles, for different λ values, can be seen in Figures 9. It is interesting to note that the λ values for which the reduction in wake width is greatest are around the point of maximum C_P.

Trends in wake width with λ are still apparent when the maximum shear method is used, however, due to the convergence difficulties associated with this method, the differences are less clear. There are two distinct regions: z/D< 5 and z/D> 5. The reason for this is again the wake shape, being either an inverted top-hat, or approximately v-shaped. $\lambda \geq 3.0$ exhibit the inverted top-hat profile until z/D ~ 5, hence the width using the maximum-shear method is well defined. Beyond this point, the profiles become v-shaped; this means there is a large cross-stream extent with an almost identical amount of shear, which itself is approximately the maximum-shear in the wake. Any slight changes in the profiles can radically change the measured width, explaining the fluctuations visible in the region z/D> 5.

All three metrics demonstrate a clear impact of tip-speed ratio on wake width, with the high λ values, high thrust cases demonstrating a wider wake. An increase in width with increasing turbine thrust can be explained by the increase in resistance to the flow causing more of the flow to be divert outwards and around the swept area of the turbine, creating a wider wake.

7.6 CFD

The low-turbulence flume tests found that the CFD overpredicts TI in the near wake region. However, from z/D= 9 to the end of the available flume data the agreement is very good, and an extrapolation of the results from the flume would show good agreement with the CFD from this point onwards, suggesting that the CFD accurately reproduces the wake by this point. Part of the reason for the over prediction of TI in the near wake will be down to the CFD's slight under-prediction of velocity recovery in this region (Figure 11a), meaning that the same magnitude of fluctuations would yield a higher value of TI. However, this is not enough to

completely explain the difference. The poor agreement in the near-wake may be improved by further increasing the mesh density, or by further investigation into possible flow separation as the blade boundary layer transitions from being laminar to being turbulent.

Good agreement between flume and CFD from z/D ~ 4 onwards was found using the fine grid. The CFD does reproduce the trend in the near-wake of the flume results and a dependence of TI on λ. Further upstream, the CFD tends to overpredict the TI. The CFD reproduces both the trend of lower λ values producing the highest initial TI, but also that any difference between these cases becomes indistinguishable from z/D ~ 4.

Good agreement was also found between flume and CFD using the coarse grid throughout the region. However, neither the flume data nor the CFD results demonstrated a dependence of wake TI on λ.

Centreline wake L_t has been validated using data from the low-turbulence flume test. As for the TI the CFD tends to overpredict L_t in the near- and mid-wake regions, but agreement is good from z/D ~ 9 onwards. As with TI, it is thought that the poor agreement in the near-wake may be improved by increasing mesh density in the region surrounding the turbine.

The CFD results for the fine grid, for $\lambda = 2.5$ and $\lambda = 3.65$, reflect the trend in the flume results of a gradual rise in L_t as the wake develops, but show an under-prediction in the rate of increase. Larger changes in $\lambda = 4.5$ indicate a possible convergence issue; other studies have shown that a sample time of 50 s is at the lower bound of what is required to obtain reliable well converged results for a higher order statistic such as integral length scale, in flows of this nature using a sample rate similar to the 200 Hz used in this study [46]. As the smallest time scales were typically approximately 0.2 s, a sample rate of 200 Hz was more than adequate to accurately capture these fluctuations.

The CFD results for the coarse grid for the three λ values modelled show similar values, in the wake, of L_t ~ 0.25 m, which remains nearly constant throughout the wake, in contrast to the steady increase of L_t seen in the flume results. The agreement is good in the near-wake region, but deteriorates as the wake develops, indicating a general trend in the CFD to under-predict length scale. The value of L_t in the CFD models for the coarse grid cases is slightly higher than those found in the fine grid cases, which reflects the trend between in the flume results. More detailed explanations can be found in Ebdon [51].

7.6.1 Impact of turbulence on wake turbulence characteristics

7.6.1.1 Turbulence intensity

The impact of ambient TI on wake centreline TI was analysed using four CFD cases. The results indicated a possible weak dependence of wake TI on ambient TI, with a higher ambient TI leading to a higher wake TI. This agrees with the mild dependence on ambient TI found in the flume results. The largest difference between the cases was in the near- to mid-wake region; by z/D= 10, there is little difference in the centreline turbulence intensities, regardless of the ambient TI upstream.

In general, there is little difference between the cases, with all cases showing a slight increase in length scale with increasing downstream distance. Both the trends in, and the magnitudes of L_t, are similar for all cases, indicating that ambient TI has little dependence on wake L_t.

7.6.1.2 Turbulence length scale

The ambient L_t on wake centreline TI was assessed through three CFD runs with identical λ values, similar TIs, but differing L_t values. No clear trend was observed, although it could be said that the cases with the shortest and longest values of ambient L_t show similar behaviours, with the medium L_t showing a significantly lower initial TI. This could indicate a non-linear response of wake centreline TI to L_t, for example suggesting that wake mixing might not simply

increase or decrease with increasing ambient L_t, but rather that there might be a value of ambient L_t which causes most mixing, and a longer or shorter L_t leads to reduced wake mixing.

The effect of ambient L_t was that in all cases a sharp initial rise in L_t was found followed by a reduction, before resuming a steady rise towards the far wake. All cases show similar results beyond approximately z/D= 10. Here there appears to be some dependence of wake L_t on ambient L_t. Possibly a larger ambient L_t leads to a larger value of L_t in the near- to mid-wake, but it also seems to cause the point at which L_t peaks before reducing to move further downstream.

7.7 Impact of tip-speed ratio on wake turbulence characteristics

The impact of λ on centreline TI was examined via seven different CFD cases in a low-turbulence environment of approximately 1.5%. The lowest λ values (λ = 1.5 and λ = 2.5) initially demonstrated a very high initial TI, which very quickly drops. λ values around the point of peak CP (λ = 3.65; 4.0; 4.5) start at approximately 25% at z/D= 2, rising to approximately 30% at z/D= 5, before reducing as the downstream distance increases further. This initial increase in TI followed by a decrease has been observed in studies such as that by Maganga et al. [13] and Baba-Ahmadi and Dong [57], and is thought to be due to the shear layers from either side of the wake merging in the centre. The high initial L_t for the lowest values of λ may be due to blade stalling changing the characteristics of the turbulence in these cases; two λ values are within or close to the stall region. The initial high TI followed by a rapid reduction in the λ = 1.5 case may be related to the rapid centreline wake recovery in this case: a higher level of turbulence promoting more rapid mixing and wake recovery

For array designers concerned with the placement of turbines, the region of increased TI in the near wake will be of some interest, however it is unlikely to be of great relevance if the turbines are to have a longitudinal spacing of more than approximately z/D= 8, or even possibly less in conditions of higher ambient turbulence. Perhaps of more interest would be that, from z/D ~ 10, λ (and therefore turbine operating condition) has little impact on wake TI.

The centreline turbulence length scale, L_t, for each of the λ values, used in the low-turbulence CFD case, generally displayed a gradual increase value as the wake develops. This is consistent with that seen in the flume results and is due to the smaller length scales dissipating due to viscous forces, leaving larger length scales dominant. However, there is a significant difference between the cases in their initial behaviour, with some cases showing an initial increase in L_t, followed by a comparable decrease, before gradually increasing once more. This complex behaviour initially appears to be linked to C_P, as tip-speed ratios with higher values of C_P appear to show a larger initial increase than those with a lower value of C_P. However, the representative length scales of the dominant turbulent features might be dependent on the rotational frequency of the turbine, rather than the operational condition (i.e. where it is operating on the curves of C_P, C_T and C_θ). The ambient L_t in these cases is approximately 0.8 m, meaning that L_t downstream of the turbine is much smaller than upstream of it. The presence of the turbine leads to a reduction in length scale, which may be caused by large turbulent features being broken up by their passage through the rotating turbine blades. The greater the rotational frequency, the smaller the resultant turbulent features, explaining why higher λ values have a smaller initial length scale. The exceptions to this, λ = 1.5 and λ = 2.5, may not fit this pattern due to the blade-stall effects discussed above. A stalled blade can be expected to produce turbulence with different characteristics to that of an unstalled blade, with effects such as flow separation leading to higher wake TI, which could explain the differences between these two cases. This more complex behaviour is only apparent in the near wake, however; from z/D~ 10, the length scales become similar regardless of λ, suggesting that it need not be considered for array layouts for $z/D \geq 10$.

8 CONCLUSIONS

Impact of turbulence on:

- ***Performance***

For all tip-speed ratios, an increase in turbine characteristics and magnitude of fluctuations is seen at higher turbulence intensities. Turbulence length scale seems to have little impact.

- ***Wakes***

Turbulence intensity was found to strongly impact wake recovery, both centreline and volumetric averaged velocity. An increase in TI always led to increased recovery, there is some suggestion that, beyond the near wake, turbulence intensities above 10% have similar results. Turbulence intensity has an impact on wake width. An increase in TI causes the fixed-threshold width to narrow, but the full-width half-minimum and maximum-shear widths to widen. Taken together, this indicates that the overall wake width is increasing, but that the region strongly impacted by the wake is decreasing. Finally, turbulence length scale was not found to have a strong impact on turbine wakes.

Wake width metrics

The fixed-threshold and full-width half-minimum methods were found to be less sensitive to wake shape than the maximum shear method, with each providing subtly different information about the wake. Due to the way these metrics complement each other, providing a more complete picture of the nature of the wake when used together, the authors recommend that both are used in future studies.

The impact of operating condition on wakes

Turbine operating condition strongly impacts the wakes of tidal turbines, although with the exception of the impact on wake width, these differences become small by ~z/D= 10.

The turbine operating condition has been shown to have an impact on wake width, with wider wakes occurring as turbine thrust increases. This impact can be seen throughout the wake length.

Implications for tidal turbine arrays

The ambient TI of a site must be taken into account for the placement of turbines in an array.

The relationship between TI and wake recovery and wake width suggests that, for an array site with higher ambient TI, longitudinal spacing may be reduced, while lateral spacing may need to be increased due to the widening of the overall area affected by the wakes.

Arrays of turbines designed to maintain rated power through overspeed will require a greater lateral spacing as both the overall width of the region affected by the wake, as well as the width of the region most heavily impacted, increase with greater C_T.

Acknowledgements

The authors acknowledge the financial support provided by:

- The Welsh Government and Higher Education Funding Council for Wales through the S*ê*r Cymru National Research Network for Low Carbon, Energy and the Environment.
- EPSRC EP/N020782/1, Dynamic Loading on Turbines in a tidal array (DyLoTTA).
- Access to IFREMER flume was funded through an EPSRC IAA and IFREMER. The authors would like to thank the staff at IFREMER for their expertise and support during the testing.
- The supercomputing facilities at Cardiff University operated by Advanced Research Computing at Cardiff (ARCCA) on behalf of the Cardiff Supercomputing Facility and the

HPC Wales and Supercomputing Wales (SCW) projects. The latter is part-funded by the European Regional Development Fund (ERDF) via the Welsh Government.

References

1 G. Pinon, P. Mycek, G. Germain, and E. Rivoalen, "Numerical simulation of the wake of marine current turbines with a particle method," *Renewable Energy*, vol. 46, pp. 111 – 126, 2012.

2 Lewis, M., Neill, S.P., Robins, P., Hashemi, M.R. and Ward, S. "Characteristics of the velocity profile at tidal-stream energy sites." *Renewable Energy*, 114, pp.258-272, 2017.

3 Togneri, M., Lewis, M., Neill, S. and Masters, I. " Comparison of ADCP observations and 3D model simulations of turbulence at a tidal energy site." *Renewable Energy*, 114, pp.273-282, 2017.

4 Lewis, M., McNaughton, J., Márquez-Dominguez, C., Todeschini, G., Togneri, M., Masters, I., Allmark, M., Stallard, T., Neill, S., Goward-Brown, A. and Robins, P. "Power variability of tidal-stream energy and implications for electricity supply." *Energy*, 183, pp.1061-1074, 2019.

5 C. H. Frost, P. S. Evans, M. J. Harrold, A. Mason-Jones, T. O'Doherty and D. M. O'Doherty, "The impact of axial flow misalignment on a tidal turbine," *Renewable Energy*, vol. 113, pp. 1333 - 1344, 2017.

6 A. Mason-Jones, Performance assessment of a Horizontal Axis Tidal Turbine in a high velocity shear environment. PhD thesis, School of Engineering, Cardiff University, 2010.

7 Y. Zhang, J. Zhang, Y. Zheng, C. Yang, W. Zang, and E. Fernandez Rodriguez, "Experimental Analysis and Evaluation of the Numerical Prediction of Wake Characteristics of Tidal Stream Turbine," *Energies*, vol. 10:2057, 2017.

8 P. Lissaman, "Energy effectiveness of arbitrary arrays of wind turbines," *J. Energy*, vol. 3, no. 6, pp. 323–328, 1979.

9 N. Jensen, "A note on wind generator interaction," tech. rep., Risø National Laboratory, Denmark, 1983.

10 S. Frandsen, R. Barthelmie, S. Pryor, O. Rathmann, S. Larsen, J. Højstrup, and M. Thøgersen, "Analytical modelling of wind speed deficit in large offshore wind farms," *Wind Energy*, vol. 9, no. 1-2, pp. 39– 53, 2006.

11 M. Bastankhah and F. Port´e-Agel, "A new analytical model for wind turbine wakes," *Renewable Energy*, vol. 70, pp. 116 – 123, 2014. Special issue on aerodynamics of offshore wind energy systems and wakes.

12 W.-H. Lam and L. Chen, "Equations used to predict the velocity distribution within a wake from a horizontal-axis tidal-current turbine," *Ocean Engineering*, vol. 79, pp. 35–42, 2014.

13 F. Maganga, G. Germain, J. King, G. Pinon, and E. Rivoalen, "Experimental characterisation of flow effects on marine current turbine behaviour and on its wake properties," *IET Renewable Power Generation*, vol. 4, pp. 498–509, November 2010.

14 W.-H. Lam, L. Chen, and R. Hashim, "Analytical wake model of tidal current turbine," *Energy*, vol. 79, pp. 512 – 521, 2015.

15 P. Mycek, G. Germain, B. Gaurier, G. Pinon, E. Rivoalen, "Numerical and experimental study of the interaction between two marine current turbines" *International Journal of Marine Energy*, Vol. 1, pp 70-83, 2013

16 M. E. Harrison, W. M. J. Batten, L. E. Myers, and A. S. Bahaj, "Comparison between CFD simulations and experiments for predicting the far wake of horizontal axis tidal turbines," *IET Renewable Power Generation*, vol. 4, pp. 613–627, November 2010.

17 R. Malki, A. Williams, T. Croft, M. Togneri, and I. Masters, "A coupled blade element momentum – Computational fluid dynamics model for evaluating tidal stream turbine performance," *Applied Mathematical Modelling*, vol. 37, pp. 3006–3020, 2013.

18 G. Bai, J. Li, P. Fan, and G. Li, "Numerical investigations of the effects of different arrays on power extractions of horizontal axis current turbines," *Renewable Energy*, vol. 53, pp. 180–186, 2013.

19 T. Nishino and R. H. Willden, “Effects of 3-D channel blockage and turbulent wake mixing on the limit of power extraction by tidal turbines,” *International Journal of Heat and Fluid Flow*, vol. 37, pp. 123–135, 2012.

20 A. Bahaj and L. Myers, “Shaping array design of marine current energy converters through scaled experimental analysis,” *Energy*, vol. 59, pp. 83– 94, 2013.

21 P. Mycek, B. Gaurier, G. Germain, G. Pinon, and E. Rivoalen, “Experimental study of the turbulence intensity effects on marine current turbines behaviour. part I: One single turbine,” *Renewable Energy*, vol. 66, pp. 729–746, 2014.

22 B. Morandi, F. D. Felice, M. Costanzo, G. Romano, D. Dhom´e, and J. Allo, “Experimental investigation of the near wake of a horizontal axis tidal current turbine,” *International Journal of Marine Energy*, vol. 14, pp. 229–247, 2016.

23 S. Tedds, I. Owen, and R. Poole, “Near-wake characteristics of a model horizontal axis tidal stream turbine,” *Renewable Energy*, vol. 63, pp. 222– 235, 2014.

24 J. Schluntz and R. Willden, “The effect of blockage on tidal turbine rotor design and performance,” *Renewable Energy*, vol. 81, pp. 432–441, 2015.

25 S. R. Turnock, A. B. Phillips, J. Banks, and R. Nicholls-Lee, “Modelling tidal current turbine wakes using a coupled RANS-BEMT approach as a tool for analysing power capture of arrays of turbines,” *Ocean Engineering*, vol. 38, pp. 1300–1307, 2011.

26 R. Malki, I. Masters, A. J. Williams, and T. N. Croft, “Planning tidal stream turbine array layouts using a coupled blade element momentum computational fluid dynamics model,” *Renewable Energy*, vol. 63, pp. 46– 54, 2014.

27 D. O’Doherty, A. Mason-Jones, C. Morris, T. O’Doherty, C. Byrne, P. Prickett, and R. Grosvenor, “Interaction of marine turbines in close proximity,” in *Proc. of 9th European Wave and Tidal Energy Conference (EWTEC), Southampton, UK*, 2011.

28 T. Stallard, R. Collings, T. Feng, and J. Whelan, “Interactions between tidal turbine wakes: experimental study of a group of three-bladed rotors,” *Philosophical Transactions of the Royal Society of London A: Mathematical, Physical and Engineering Sciences*, vol. 371, no. 1985, 2013.

29 M. Nuernberg and L. Tao, “Experimental study of wake characteristics in tidal turbine arrays,” *Renewable Energy*, vol. 127, pp. 168–181, 2018.

30 P. Jeffcoate, T. Whittaker, C. Boake, and B. Elsaesser, “Field tests of multiple 1/10 scale tidal turbines in steady flows,” *Renewable Energy*, vol. 87, pp. 240–252, 2016.

31 C. Morris, D. O’Doherty, A. Mason-Jones, and T. O’Doherty, “Evaluation of the swirl characteristics of a tidal stream turbine wake,” *International Journal of Marine Energy*, vol. 14, pp. 198–214, 2016.

32 P. Mycek, B. Gaurier, G. Germain, G. Pinon, and E. Rivoalen, “Experimental study of the turbulence intensity effects on marine current turbines behaviour. part II: Two interacting turbines,” *Renewable Energy*, vol. 68, pp. 876–892, 2014.

33 I. Afgan, J. McNaughton, S. Rolfo, D. Apsley, T. Stallard, and P. Stansby, “Turbulent flow and loading on a tidal stream turbine by LES and RANS,” *International Journal of Heat and Fluid Flow*, vol. 43, pp. 96–108, 2013.

34 T. Blackmore, W. Batten, and A. Bahaj, “Influence of turbulence on the wake of a marine current turbine simulator,” *Proc. R. Soc. A*, vol. 470, p. 20140331, 2014.

35 P. Ouro, M. Harrold, T. Stoesser, and P. Bromley, “Hydrodynamic loadings on a horizontal axis tidal turbine prototype,” *Journal of Fluids and Structures*, vol. 71, pp. 78–95, 2017.

36 M. Churchfield, Y. Li, and P. Moriarty, “A large-eddy simulation study of wake propagation and power production in an array of tidal-current turbines,” *Phil. Trans. R Soc. A*, vol. 371, p. 20120421, 2013.

37 C. Morris, *Influence of Solidity on the Performance, Swirl Characteristics, Wake Recovery and Blade Deflection of a Horizontal Axis Tidal Turbine*. PhD thesis, School of Engineering, Cardiff University, 2014.

38 M. Ikhennicheu, G. Germain, P. Druault, B. Gaurier, “Experimental investigation of the turbulent wake past realistic seabed elements for velocity variations characterization in the water column,” *Renewable Energy*, 2020.

39 P. Mercier, M. Ikhennicheu, P. Druault, S. Guilloux, G. Germain, “The merging of Kelvin-Helmholtz vortices into large coherent flow structures in a high Reynolds number flow past a wall-mounted square cylinder,” *Ocean Engineering*, 2020.

40 M. H. Ahmadi, “Influence of upstream turbulence on the wake characteristics of a tidal stream turbine,” *Renewable Energy*, vol. 132, pp. 989–997, 2019.

41 C. H. Frost, P. S. Evans, M. J. Harrold, A. Mason-Jones, T. O’Doherty, and D. M. O’Doherty, “The impact of axial flow misalignment on a tidal turbine,” *Renewable Energy*, vol. 113, pp. 1333–1344, 2017.

42 T. de Jesus Henriques, S. Tedds, A. Botsari, G. Najafian, T. Hedges, C. Sutcliffe, I. Owen, and R. Poole, “The effects of wave-current interaction on the performance of a model horizontal axis turbine,” *International Journal of Marine Energy*, vol. 8, pp. 17–35, 2014.

43 S. Tatum, C. Frost, M. Allmark, D. O’Doherty, A. Mason-Jones, P. Prickett, R. Grosvenor, C. Byrne, and T. O’Doherty, “Wave-current interaction effects on tidal stream turbine performance and loading characteristics,” *International Journal of Marine Energy*, vol. 14, pp. 161–179, 2016.

44 M. Allmark, *Condition Monitoring and Fault Diagnosis of Tidal Stream Turbines Subjected to Rotor Imbalance Faults*. PhD thesis, School of Engineering, Cardiff University, 2016.

45 C. Frost, *Flow Direction Effects On Tidal Stream Turbines*. PhD thesis, School of Engineering, Cardiff University, 2016.

46 T. Blackmore, L. E. Myers, and A. S. Bahaj, “Effects of turbulence on tidal turbines: Implications to performance, blade loads, and condition monitoring,” *International Journal of Marine Energy*, vol. 14, pp. 1–26, 2016.

47 T. Ebdon, D. O’Doherty, T. O’Doherty, and A. Mason-Jones. Modelling the effect of turbulence length scale on tidal turbine wakes using advanced turbulence models. In *Proc. of 12th European Wave & Tidal Energy Conference (EWTEC 2017)*, 27th Aug – 1st Sept. 2017.

48 Fredriksson, S., Broström, G., Jansson, M., Nilsson, H., & Bergqvist, B. J. M. “Large eddy simulation of the tidal power plant deep green using the actuator line method” *IOP Conference Series: Materials Science and Engineering* vol. 276(1), pp. 012014, 2017

49 Fredriksson, S. T., Brostrom, G., Bergqvist, B., Lennblad, J., & Nilsson, H. Turbulence Characteristics in Tidal Flows Using LES and ALM to Model the Tidal Power Plant Deep Green. In *Proc. of 4th Asian Wave & Tidal Energy Conference (AWTEC 2018)*, 9th-13th Sept. 2018.

50 McCaffrey, K., Fox-Kemper, B., Hamlington, P. E., & Thomson, J. “Characterization of turbulence anisotropy, coherence, and intermittency at a prospective tidal energy site: Observational data analysis.” *Renewable Energy”* vol. 76, pp. 441—453, 2015.

51 T. Ebdon, *The Impact of Turbulence and Turbine Operating Condition on the Wakes of Tidal Turbines.* PhD thesis, School of Engineering, Cardiff University, 2019.

52 H.K. Versteeg and W. Malalasekera. *An Introduction to Computational Fluid Dynamics, The Finite Volume Method*. Pearson Education Limited, 2007.

53 I.A. Milne, R.N. Sharma, R.G.J. Flay, and S. Bickerton. Characteristics of the turbulence in the flow at a tidal stream power site. *Phil Trans R Soc A*, 371:20120196, 2013.

54 T. Ebdon, D. O’Doherty, T. O’Doherty, and A. Mason-Jones. Simulating Marine Current Turbine Wakes Using Advanced Turbulence Models. In *Proc. of 3rd Asian Wave & Tidal Energy Conference (AWTEC 2016)*, 24th–28th Oct. 2016.

55 P. R. Bevington and D. K. Robinson, Data reduction and error analysis for the physical sciences. McGraw-Hill, 2003.

56 National Institute of Standards and Technology, \e-Handbook of Statistical Methods." http://www.itl.nist.gov/div898/handbook/, 2013. [Online; last accessed 23-August-2018].

57 M. H. Baba-Ahmadi and P. Dong, “Numerical simulations of wake characteristics of a horizontal axis tidal stream turbine using actuator line model,” *Renewable Energy*, vol. 113, pp. 669–678, 2017.

Appendix:

Table A.1: Turbine performance metrics, all CFD runs. The velocity used for the calculations of C_P, C_T and C_θ are the target velocities.

v / ms^{-1}	TI /%	L_t /m	λ	C_P	C_T	C_θ	σ_{C_P}	σ_{C_T}	σ_{C_θ}	run no.
1.1	5	0.25	2.5	0.35	0.67	0.14	0.0118	0.017	0.0047	1
1.1	5	0.25	3.65	0.43	0.85	0.12	0.0192	0.024	0.0052	2
1.1	5	0.25	4.5	0.41	0.89	0.09	0.0182	0.025	0.0041	3
1.1	5	0.50	2.5	0.35	0.67	0.14	0.0200	0.036	0.0080	4
1.1	5	0.50	3.65	0.44	0.86	0.12	0.0398	0.050	0.0109	5
1.1	5	0.50	4.5	0.42	0.90	0.09	0.0203	0.025	0.0045	6
1.1	5	1.00	2.5	0.35	0.67	0.14	0.0101	0.016	0.0040	7
1.1	5	1.00	3.65	0.43	0.85	0.12	0.0200	0.025	0.0055	8
1.1	5	1.00	4.5	0.41	0.89	0.09	0.0217	0.026	0.0048	9
1.1	10	0.25	2.5	0.35	0.67	0.14	0.0289	0.040	0.0116	10
1.1	10	0.25	3.65	0.41	0.82	0.11	0.0468	0.058	0.0128	11
1.1	10	0.25	4.5	0.44	0.92	0.10	0.0486	0.055	0.0108	12
1.1	10	0.50	2.5	0.34	0.66	0.14	0.0237	0.046	0.0095	13
1.1	10	0.50	3.65	0.44	0.86	0.12	0.0210	0.031	0.0057	14
1.1	10	0.50	4.5	0.44	0.93	0.10	0.0463	0.058	0.0103	15
1.1	10	1.00	2.5	0.34	0.66	0.14	0.0213	0.033	0.0085	16
1.1	10	1.00	3.65	0.43	0.85	0.12	0.0431	0.051	0.0118	17
1.1	10	1.00	4.5	0.44	0.92	0.10	0.0486	0.055	0.0108	18
1.1	20	0.25	2.5	0.36	0.70	0.14	0.0529	0.075	0.0212	19
1.1	20	0.25	3.65	0.43	0.84	0.12	0.0815	0.100	0.0223	20
1.1	20	0.25	4.5	0.43	0.91	0.10	0.1086	0.126	0.0241	21
1.1	20	0.50	2.5	0.33	0.65	0.13	0.0407	0.061	0.0163	22
1.1	20	0.50	3.65	0.50	0.91	0.14	0.1304	0.151	0.0357	23
1.1	20	0.50	4.5	0.44	0.92	0.10	0.1121	0.135	0.0249	24
1.1	20	1.00	2.5	0.33	0.65	0.13	0.0447	0.081	0.0179	25
1.1	20	1.00	3.65	0.42	0.83	0.12	0.0878	0.107	0.0241	26
1.1	20	1.00	4.5	0.40	0.88	0.09	0.0653	0.080	0.0145	27
1.02	11.7	0.19	2.5	0.33	0.66	0.13	0.0365	0.070	0.0146	28
1.02	11.7	0.19	3.65	0.44	0.85	0.12	0.0678	0.090	0.0186	29
1.02	11.7	0.19	4.5	0.42	0.90	0.09	0.0802	0.102	0.0179	30
1.03	17.5	0.43	2.5	0.34	0.68	0.14	0.0728	0.136	0.0292	31
1.03	17.5	0.43	3.65	0.45	0.86	0.12	0.1105	0.144	0.0303	32
1.03	17.5	0.43	4.5	–	–	–	–	–	–	33
1.5	1.75	0.50	1.5	0.14	0.49	0.10	0.0028	0.010	0.0019	34
1.5	1.75	0.50	2.5	0.35	0.67	0.14	0.0074	0.010	0.0030	35
1.5	1.75	0.50	3	0.42	0.79	0.14	0.0062	0.009	0.0021	36
1.5	1.75	0.50	3.65	0.44	0.86	0.12	0.0081	0.010	0.0022	37
1.5	1.75	0.50	4	0.44	0.88	0.11	0.0148	0.017	0.0037	38
1.5	1.75	0.50	4.5	0.42	0.90	0.09	0.0158	0.018	0.0035	39
1.5	1.75	0.50	5.5	0.33	0.90	0.06	0.0164	0.019	0.0030	40